Smart Agricultural Technology 3 (2023) 100109

Contents lists available at ScienceDirect

Smart Agricultural Technology

journal homepage: www.journals.elsevier.com/smart-agricultural-technology

Indwelling robots for ruminant health monitoring: A review of elements

Upinder Kaur [a,1,*], Rammohan Sriramdas [b,1], Xiaotian Li [b], Xin Ma [a], Arunashish Datta [c], Barbara Roqueto dos Reis [d], Shreyas Sen [c], Kristy Daniels [b], Robin White [b], Richard M. Voyles [a,*], Shashank Priya [b]

[a] School of Engineering Technology, Purdue University, West Lafayette, IN 47907, United States
[b] Materials Research Institute, Pennsylvania State University, University Park, PA 16802, United States
[c] Elmore Family School of Electrical and Computer Engineering, Purdue University, West Lafayette, IN 47907, United States
[d] Animal and Poultry Sciences, Virginia Tech, Blacksburg, VA 24061, United States

ARTICLE INFO

Keywords:
Rumen health
Indwelling robot
Locomotion
Localization
Wireless power transfer
Wireless data transmission
Ruminants
Health monitoring

ABSTRACT

Maximizing the health, productivity, and sustainability of ruminant animals is an essential societal goal for a variety of reasons including food security, impact on the environment, and global nutrition; however, monitoring the metabolism of ruminant animals is currently a time-consuming and imprecise process. An indwelling robot residing within the ruminant gut would likely revolutionize metabolic monitoring in ruminants by providing a new level of detail into the complex and stratified chemistry of fermentation that goes on hour by hour. Indwelling robots could become an essential tool for ruminant health monitoring because many of the health, productivity, and sustainability challenges experienced by ruminants can be indicated and potentially influenced by changes in biomarkers within the rumen. We believe next-generation ruminant health monitoring will evolve from continuous biomarker measurement, reliable data transmission, and precise locomotion, all of which can be enabled by advances in indwelling ruminal robot design. Within this review, we summarize the requirements of and progress toward engineering advancements necessary to develop field-deployable robots for ruminant metabolic monitoring. The vital elements of an autonomous indwelling medical robot include locomotion, localization, wireless data transmission, and wireless power transfer. The state-of-the-art technologies associated with each element are articulated in this review. The comprehensive techniques of locomotion, the approaches for precise localization, as well as technologies for wireless power and data transmission that will make the indwelling robot entirely autonomous are enunciated, with a special focus on ruminants. The evaluated indices are potentially useful not only to assess the health of the ruminant but also to refine and standardize the assessment protocols. The overview presented in this article on the advances, imperative requirements, and challenges enables the deployment of the ruminal robot for health monitoring in ruminants.

Introduction

As the world prepares for a food safety challenge for a population approaching 10 billion by 2050 [1], the need is to improve the productivity of existing agricultural systems in the face of decreasing land availability, water scarcity, and degrading soil quality. The food consumption rise is not projected to be uniform across dietary categories as growing populations demand more animal-based proteins, with the demand for dairy rising by 8.9% by 2050 in the United States alone [2]. However, the already stressed business of dairy farming faces challenges of ethical treatment, animal welfare, and global climate impact while improving overall productivity and sustainability [3]. Therefore, the need is to improve the efficiency and productivity of dairy farming operations while focusing on the health and welfare of individual animals.

The health, productivity, and sustainability of dairy cattle are closely tied to the rumen – a primary digestive chamber. The rumen comprises a highly stratified environment with a gaseous volume at the top, followed by a thick mat of fresh feed that floats on top of a liquid volume that converts largely human-indigestible plant proteins into human-digestible animal proteins through fermentation. The rich biodiversity of microbes that line the walls of the rumen help converts feed into volatile fatty acids which act as the main source of energy for the animal.

* Corresponding author.
E-mail addresses: kauru@purdue.edu (U. Kaur), rvoyles@purdue.edu (R.M. Voyles).
[1] Equal first author credit.

https://doi.org/10.1016/j.atech.2022.100109
Received 1 January 2022; Received in revised form 16 May 2022; Accepted 15 August 2022
Available online 17 August 2022

Numerous biomarkers in the rumen indicate the overall health of the animal and its productivity while modulating the outputs that impact the environment. However, current methods of monitoring the rumen rely on surgically-created cannula ports to access the ruminal contents, which are only feasible for a tiny fraction of any herd. These methods not only introduce oxygen into a naturally anaerobic environment but also impede the study of interlayer interactions. Hence, the need is for an active mobile sensor that can locomote in the rumen and wirelessly communicate important biomarker information in real-time without impacting the animal's health. A soft robot with active sensing seems to be the optimal solution to the problem.

Recent years have witnessed accelerated development in advanced robotics for nearly innumerable applications. In the field of bio-inspired robotics, fundamental principles of a given biological system are first studied, and then key processes are translated and incorporated into robot design, creating a robot that performs tasks like a natural system element [4]. Bio-inspired robots have been around since at least the 1940s when W. Grey Walter made robotic turtles to demonstrate his theories of the human nervous system [5]. Over time, diversity in types of bio-inspired and bio-compatible robots has increased and this review will highlight how these developments and applications can be leveraged to better study the rumen.

One of the most applicable advances in the development of bio-inspired and bio-compatible robotics is that of soft robots. Soft robots, consisting of flexible structures, perform specific tasks that would be difficult to achieve or would be unreasonably damaging with conventional robots fabricated from rigid materials [6]. Rigid materials are often incompatible with many biological applications because they induce damage and restrict the characteristics of soft tissues, effectively providing an "impedance mismatch" at the interface between the mechanism and biological tissue [7,8]. By comparison, soft robots are composed of soft and extensible materials [9] and are able to bend and twist with high curvatures, can be incorporated in confined spaces [10], and have the ability to adapt to their environment [11] without harming living tissue. Moreover, locomotion movements such as walking, running, climbing, swimming, flying, and crawling, can be utilized in soft robotic structures [12]. It is these advancements in robotics that create opportunities to apply robotics science within the animal sciences.

The applicability of soft bioinspired robots goes beyond locomotion, as their beneficial characteristics have been applied throughout the medical field, e.g. in implants [13], minimally invasive surgery [14], wearables [15], and therapeutic technologies [16,17]. Implantable sensors, such as those used for the regeneration of the gastrointestinal tract in humans, have the capacity to assist in the whole process of repair and regeneration of the tissue of interest by using remote communication [18]. The bionic implant is another example and functions as the replacement for different affected organs such as the heart [19], esophagus [18], or pancreas [20]. While no such robot exists for direct application inside the rumen, in this work we analyze the published literature for all necessary elements of such a robot.

The critical elements of medical robots for monitoring and mapping the rumen include locomotion, localization, wireless power transfer, and wireless communication. Mapping the rumen requires effective locomotion and localization of the robot to purposefully traverse the entire rumen volume with a suitable metabolic sensor payload. (Recent reviews of sensors for ruminant metabolism include a companion to this paper in [21] and one by Knight in [22].) The data generated by the sensors need to be communicated out of the body wirelessly to support actionable plans. Further, to extend the life of the robot, wireless power transfer can be used. In subsequent sections, we first explain the rumen environment and then discuss the literature for each of the previously stated elements. We identify possible approaches and their extensions that can help address the challenges posed by the ruminal environment.

The rumen ecosystem and the need for indwelling robotics

The rumen is the largest compartment of the ruminant's stomach and the primary site of fermentation in ruminants. Ingested nutrients, such as fiber, starch, sugar, and proteins, are fermented by the microbes and converted to alternative proteins that are digestible by humans. As the product of the fermentation process, volatile fatty acids, which are the main energy sources for the ruminant, are produced and absorbed. Therefore, monitoring the rumen environmental conditions is essential as they indicate the digestive functionality of the animal as well as its immediate health status. Yet, static sensors, used presently, are not enough. The rumen environment is highly stratified so mobility is a key element in gathering accurate data from all levels of the digestive process. In addition, static sensors are naturally collected by the reticulum, over time, rendering them of marginal value. Therefore, the potential of a robotic, metabolic, active sensor platform to provide continuous, uncompromised, longitudinal data for the unprecedented study and manipulation of the health, productivity, and sustainability of animal herds seems extraordinarily high.

Among the numerous rumen environmental variables, ruminal pH value has been considered as the most important phycological parameter, to date, because it not only particularly affects the nutritional status of ruminant livestock but also indicates the functional status of the rumen [23,24]. An example of the interaction between health and productivity is sub-acute ruminal acidosis (SARA) in dairy cows, a digestive disorder that has no typical clinical signs, but can result in feed intake depression, low milk yield, injury to the gastrointestinal lining, and a host of other negative outcomes. In the delicate balance to maximize production to meet growing demand, SARA can result from over-feeding of grain diets that are high in starch and low in fiber but increase milk production. SARA has emerged as one of the most significant nutrition-related problems in the dairy industry, resulting in economic losses worth $1 billion each year in the US, alone. SARA occurs in an environment in which the ruminal pH value falls below 5.5 [25]. In the case of healthy ruminant livestock, the ruminal pH value determined by the dynamic balance between the intake of fermentable carbohydrates, the buffering capacity of the rumen, and the rate of acid absorption from the rumen is maintained between 5.5 and 7.0 [26]. But, unbalanced nutrient intake, such as high levels of fast digestible carbohydrates, lowers the pH value of the rumen below 5.5. As such, it is important to continuously monitor the ruminal pH value and discern the change in its value on a timescale of hours. An indwelling robot with pH and temperature sensing capability would be able to notice this change across the stratified layers of the rumen and help in the timely identification of the onset of SARA. Additionally, intestinal mechanical activity is an indication of gastrointestinal (GI) motility. The GI motility in cattle is affected by several conditions such as GI obstruction, diarrhea, hypocalcemia, and pregnancy [27]. The normal ruminal motility in cattle is a sign of healthy GI motility. The normal ruminal motility serves to mix the ingesta, eructate gas, and propel fermented food into the omasum. When the ruminal contents become acidic, the motility ceases due to a decrease in the protozoal population [28]. Hence, active monitoring of pH levels is crucial to ensure ruminal wellbeing and productivity.

The principal volatile fatty acids that collectively provide the energy needs in the rumen include acetic, propionic, and butyric acids with an approximate molar ratio of 70:20:10. Simultaneously, 30-50 liters of gases that include carbon dioxide and methane are released after fermentation. The disruption in the normal eructation of these gases can be life-threatening to ruminants as it interferes with lung function. Other severe factors affecting the GI tract include hypocalcemia and hypokalemia. The serum biochemical analysis is required when GI stasis is indicated by the sensors. Although volatile fatty acids and pH are the significant parameters of interest, other parameters such as methane, sodium, oxygen, and potassium provide vital information about the health of the rumen. Methane, in particular, is a parameter of great

interest due to climate change impact. Recent studies have shown correlations between the rumen microbiome structure and methane output [29,30]. Adjusting the rumen microbiome using additives, such as linseed oil, can help reduce methane output without affecting the animal's health as methane by itself is not useful for the animal [29]. An indwelling robot equipped with the ability to continuously monitor these parameters will be an invaluable tool to assess animal health as well as aid in measuring the impact of additives on ruminal processes.

Taking the parameters of interest into account, we envision a system with an indwelling ruminal robot as shown in Fig. 1. The schematic in Fig. 1 illustrates the numerous parameters of interest and the data flow from the ruminal robot to a base station and an alert system on health indicators. An indwelling robot that is in direct contact with the ruminal fluid consists of several sensors that measure the required parameters and send the signal to a base station. The raw data is then analyzed and processed at the base station. The health indicators such as GI motility, rumination time, microbial ecosystem, nutrient synchrony, abomasal displacement, and ruminal fermentation are the key metrics used to determine rumen and digestive health. The data is monitored continuously. Any deviation from the expected bounds is treated as an alert and an appropriate beacon is activated to alarm the caregivers. While such an indwelling robot offers incredible insights into the health of the ruminants, the realization of the ruminal robot is ensnared with several technological challenges.

The key challenges to address the implementation of indwelling ruminal robots include- (1) the ability to propel through the ruminal fluid. The entire volume of the rumen is highly stratified with gases on the top, followed by a thick mat of fibers which then gives way to a liquid of varying particle sizes that is almost clear at the bottom. (2) The knowledge of the precise location of the robot within the rumen is essential. The capacity of a rumen of an adult cow can be up to 184 liters. As the location of measurement largely governs the repeatability, the localization of the ruminal robot is a vital functionality. (3) The capability to compute and transmit the data wirelessly is another key element of the ruminal robot, as oxygen should not be introduced to facilitate measurement. The interaction between these three constituent challenges contributes to functions such as navigation, data acquisition (monitor), and control. The coordination among the three elements is depicted in Fig. 2 (a). It may be noted that control is an integral element of the ruminal robot as it derives inference from the localization elements to control the locomotion while driving the communication. The objective of this review is to summarize recent advancements in bioinspired robotics, with specific emphasis on relevant innovations in locomotion, localization, power, and wireless data transmission that are vital in the development of the next generation of indwelling robotics for use in livestock species. The trend in publications (PubMed [31]) over the last three decades on cattle medical robotics, wireless endoscopic pill-cam, and wireless medical robotics is shown in Fig. 2 (b). It may be noted from a slowly increasing publication trend of cattle medical robotics that several challenges associated with locomotion, localization, and wireless data transmission need to be addressed. The state-of-the-art innovations in each of these elements and the future directions for the implementation of a ruminal robot will be articulated in this article.

Locomotion of Rumen robot

The rumen of a cow is essentially a large fermentation vat that rhythmically contracts to churn digesta for optimum digestion. The walls of the rumen are covered with finger-like projections, called rumen papillae, which are responsible for the absorption of nutrients. This vast and dynamic space full of a variety of particles presents unique challenges for the locomotion of an indwelling robot. Potentially, promising locomotion designs for such an exceptional environment can be crawling and swimming motions. The crawling robots inspired by animal locomotion have made enormous progress over the past two decades.

Most bioinspired mobile robots are built with the characteristic of autonomous motion, decision-making capability, and environment adaptability observed in animals. Replicating the motion observed in animals with and without internal skeletons can similarly be categorized into the following two groups: hard robots and soft robots. Both kinds of robots have their merits and demerits based on the complexity of the

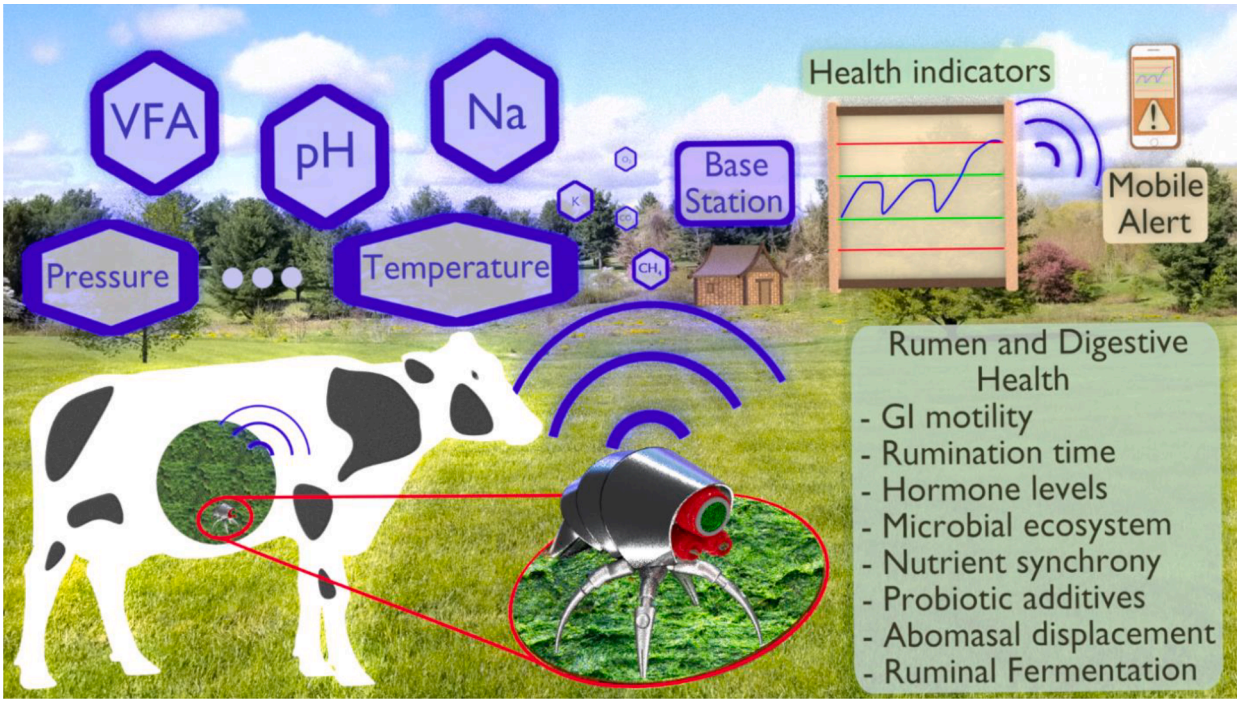

Fig. 1. A schematic of the potential of indwelling ruminal robot. The raw data from the ruminal robot after analyzing the rumen contents is wirelessly sent to a base station. The base station processes the received data and assesses the digestive health by monitoring health indicators. Any deviations from the standard trend would be communicated as an alert through a beaconing system.

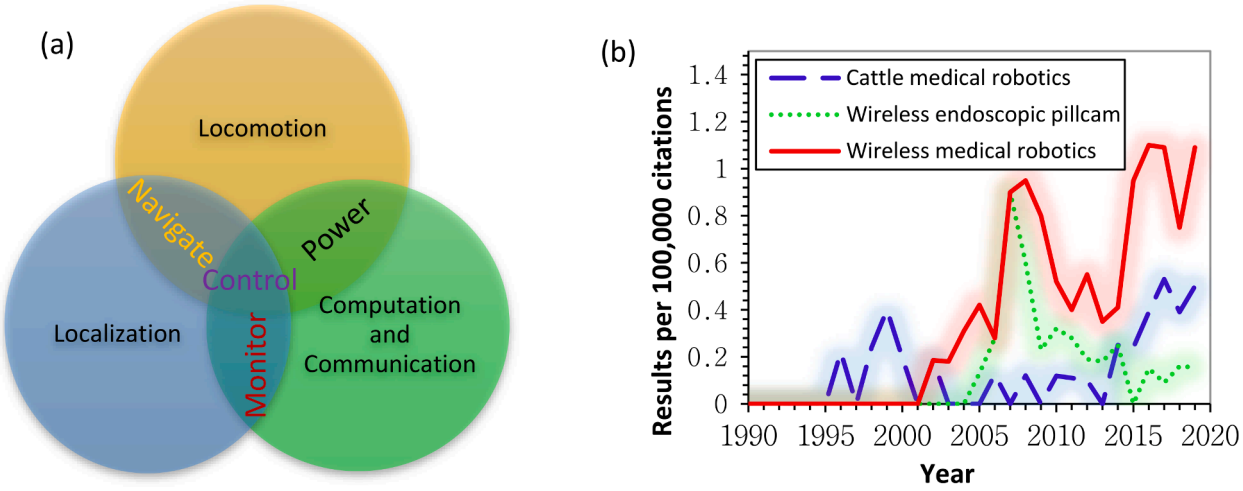

Fig. 2. (a) The three key elements of an indwelling ruminal robot are 1. Locomotion, 2. Localization and 3. Computation and communication. Control is central to all the elements of the robot. The functional interaction between the individual elements is also shown. (b) The publication trend for cattle medical robotics is compared with wireless medical robotics derived from the data on PubMed at https://esperr.github.io/pubmed-by-year

functions and possible motions. A review of the bioinspired hard and soft robots with a special focus on the challenges to implementing them in the ruminal environment is discussed below.

Hard robots are predominantly conventional machines equipped with wheels or treads for mobility. The hard robots are often built replicating the conceptual gait models observed in animals with skeletons using hard materials and structures. The range of actuation, stability, and control are some of the significant parameters in hard robots. The robots simulating the motion of *C. elegans*, razor clam, mole crab, earthworm, inchworm, spider, starfish, etc., are studied by several researchers, and considering their size, complexity and possible motions, the locomotion mechanism adopted in these robots could be a potential candidate for rumen robot. A rumen robot is expected to perform not only crawling and burrowing but also swimming to move through the stratified layers of the ruminal contents. Hence, the hard robotic concepts that are directly applicable to achieve locomotion in rumen robots are discussed in detail in the following sub-sections.

The motion observed in *Caenorhabditis elegans* and *Ensis directus* are directly applicable to the rumen robot as these animals can move through the viscous medium and soil with relative ease (Fig. 3 (a)). In [32], the motion of *C. elegans* is simulated by a series of rigid links connected by an actuator. The actuator consists of a shape memory alloy (SMA) spring connected in parallel with a passive spring. The thermally actuated SMA is selected as it offers up to 50% deformation compared to the original length in the coiled spring-like configuration. It is shown that a 12 segmented robot closely mimics the motion in *C. elegans* with

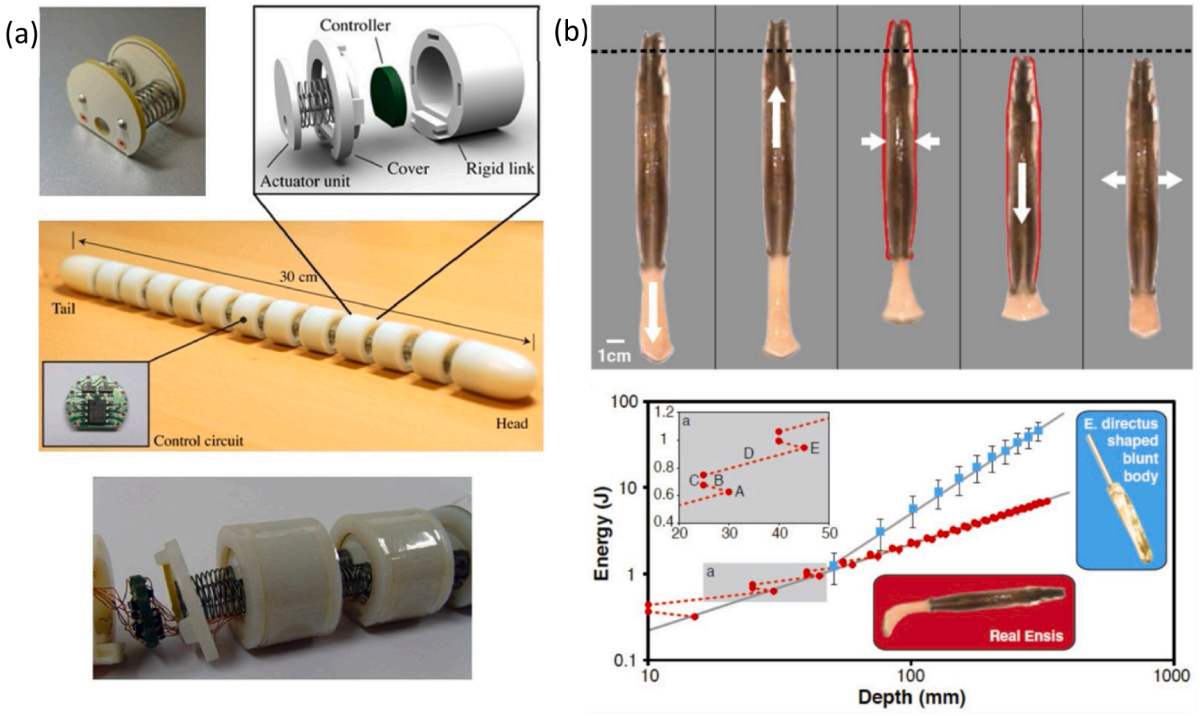

Fig. 3. (a) The crawling robot assembly consisting of an SMA and a passive spring arrangement connecting rigid links along with a control circuit simulating *C. elegans*. [32] (b) Digging cycle kinematics and energetics in Ensis directus. The energetics associated with a real Ensis is compared with a blunt body with depth. [33].

an undulation frequency of 0.17 Hz. The effect of different wall frictional anisotropy on the forward motion is evaluated experimentally, however, a shorter length would be preferable for a rumen robot.

An interesting technique adopted by the Atlantic razor clam, *Ensis directus*, reduces the energy required to dig into submerged soil [33] as shown in Fig. 3 (b). The razor clam generates 10 N force to move through the soil using as low energy as 0.27 J/cm with digging depths up to 70 cm. In order to achieve this, *E. directus* fluidizes the soil converting the dry soil into the viscous Newtonian fluid that drastically reduces the drag. Optimization of the digging cycle parameters results in specific contraction and expansion times of the Robo-Clam [34]. It is observed that the speed of landslide collapse in normally consolidated soils is independent of the depth while the speed of annular collapse in over-consolidated soils increases with the depth. The study indicated that the target zero-stress state governing contraction times suggests the Robo-Clam can dig into dry soil as well. This could be a potential locomotion approach for rumen robots. Similarly, a burrowing robot inspired by mole crab *E. talpoida* locomotion is implemented to locate volatile chemicals released underground [35]. The prototype achieved 2 mm/s speed and 2 deg/s turning rates while burrowing through the sand. Bioinspired burrowing robots have been demonstrated in several applications including anchoring [36], oil retrieval [37], sensor placement [38], and drug delivery [39], however, compact and limbless mechanisms of the locomotion are preferred for ruminal applications.

An earthworm-inspired peristaltic crawling motion is a compact limbless locomotion approach suitable for rumen robots. The large surface of contact during locomotion and small space requirements are the key advantages of the mechanism. Several segments are connected to each other and peristalsis is introduced into the segments systematically to advance the mechanism through close contact with body tissues [40,41]. A prototype with a weight to length ratio of 0.36 g/mm weighs 220 g and achieves an average speed of up to 12.3 mm/s [42]. The earthworm-like robot for effective motion through the GI tract was studied using an in vitro prototype, and an optimum stroke length was derived based on simulations and experiments [43]. A prototype consisting of two segments with 15 mm diameter and 20 mm length is tested within an intestine wall of a 7.5 mm radius to determine the critical stroke to be 7 mm. An earthworm-inspired robot consisting of five segments with each segment weighing 50 g and spanning 37 mm x 41 mm x 31 mm is operated using solenoid actuators in [44]. The overall length of 210 mm and achieves a speed of 27.2 mm/s (0.13 body lengths per second) and 2 deg/s turning rate at 0.6 A current through a pair of solenoid plungers. Another robotic design is realized with five segments with a diameter as small as 12 mm for the human intestine and colon [45]. Each segment consumes 290 mW power for locomotion and the robot reaches an average speed of 0.16 mm/s in the colon and 0.22 mm/s in the small intestine.

The peristaltic crawling observed in earthworms is a favorable and safe form of locomotion for the ruminal robot as the limbless mechanism is harmless to the internal organs and causes less disturbance to the digesta. But the need for intimate contact with body tissues in the expansive rumen might limit locomotion throughout the rumen volume. Alternative mechanisms of locomotion providing positive traction such as that observed in the inchworm, spider or starfish offer more control when moving through the dynamic rumen environment, but can potentially introduce more harm. An inchworm-inspired crawling is achieved using differential drive soft modules (DDSM) in [46]. Although individual DDSM can achieve 9.75 mm/s and a turning rate of 1.58 deg/s, the modular DDS robot with three DDSMs in series provided steering and crawling capabilities at an average speed of 4.81 mm/s and 0.71 deg/s. A mechanism for reconfiguring between crawling, rolling, and climbing inspired by *Cebrennus rechenbergi* spider is implemented in a robot and experimentally verified [47]. The weight of the robot is 350 g with a rolling diameter of 105 mm. A starfish-inspired robot is designed for crawling and swimming using flexible rays and shape memory alloy (SMA) actuators [48]. The SMA actuated starfish robot is observed to pass an obstacle nearly twice its body height. Moreover, an average speed of 130 mm/min is achieved while crawling on sand and 20.7 mm/min while creeping on a clammy rough terrain. The overall size of the mechanism is a critical aspect of the ruminal robot to achieve the desired actuation, range, and control. The reliable and compact mechanism of locomotion in hard robots encourages their application to rumen monitoring. However, the use of rigid structures and hard materials is a major drawback, particularly for the indwelling ruminal robot.

Soft robots, on the other end, are fabricated primarily using elastomeric polymers that provide mechanical strength resembling the muscles in animals without a skeleton [49]. These robots have several advantages over hard robots. The stability when moving through different terrain, simpler control for gripping, light and inexpensive actuation mimicking natural systems, and increased safety and animal compatibility are some of the notable merits of soft robots [50,51]. The primary challenge in building soft robots is the presence of large-scale deformation in a continuum body with relatively high compliance. This deformation is critical for the ruminal robot particularly to facilitate steering capability and locomotion through the digesta providing safety to the internal organs. The conventional fabrication techniques to generate large and complex morphologies suffer from repeatability and scalability issues. In order to address these challenges, multibody robots with complex morphologies are constructed using soft-unit modules that consistently reproduce certain properties of the soft robot [9].

An autonomous soft robotic fish consisting of fluidic actuators is realized to perform rapid escape maneuvers [52]. A tail stroke frequency of 1.67 Hz resulted in a velocity of 150 mm/s. Moreover, a significant decrease in heading angle was observed by employing sequential agonistic and antagonistic actuation resulting in a double-bend escape response. The use of Pneu-net (PN) chambers (Fig. 4(a)) is a straightforward method of achieving complex locomotion including gait variations [53]. The feasible morphologies for the fluidic actuator include ribbed channel structure with embedded transmission lines, cylindrical channel structure with a hollow interior, and seamless pleated channel structure [54]. Three reliable fabrication techniques to fabricate the actuators include 1.) a lamination-based casting with heterogeneous embedded components, 2.) a retractable-pin-based casting process, and 3.) a lost-wax-based casting process. These methods provide a means of rapidly constructing arbitrary morphology using soft robots. By constructing soft unit modules and concatenating them into multi-segment structures a complex morphology can be constructed as shown in Fig. 4 (b). The linearity in the bend angle of cylindrical morphology at high inflations offers easier control of the structure. However, pleated segment morphology tolerates the highest fluidic energies offering the highest possible forces. The study of soft robots is highly encouraged by the fact that animal-robot interactions will be much safer when the compliance of the machine matches the soft biological materials [55]. Hence, soft robotics combined with a peristaltic mechanism is indispensable to realize an indwelling ruminal robot. Table 1 provides a summary of different state-of-the-art technologies that can be adapted for locomotion in an indwelling ruminal robot.

Medical microrobots in the form of wireless swimmers are examined for moving through the blood vessels. Wireless endoscopic capsules with locomotion and data transmission capability can be directly adopted to realize the ruminal robot. Microorganisms propel in a liquid medium using a method called flagellar swimming [65]. The configuration is realized using a spiral wire with a small magnetic head. The magnetic torque rotates the magnet in an alternating magnetic field. The waves along the spiral wire provide the required thrust to advance through the medium. The shape of the spiral, tail width, tail length, and frequency of excitation affects the swimming velocity. The velocity of swimmers is governed by Lighthill's theory [66]. The swimmers are tested in an environment with glycerin inside a polyvinyl chloride pipe simulating flow in blood vessels [67]. It is observed that peak swimming velocity response occurs at a lower frequency in a high viscous liquid such as

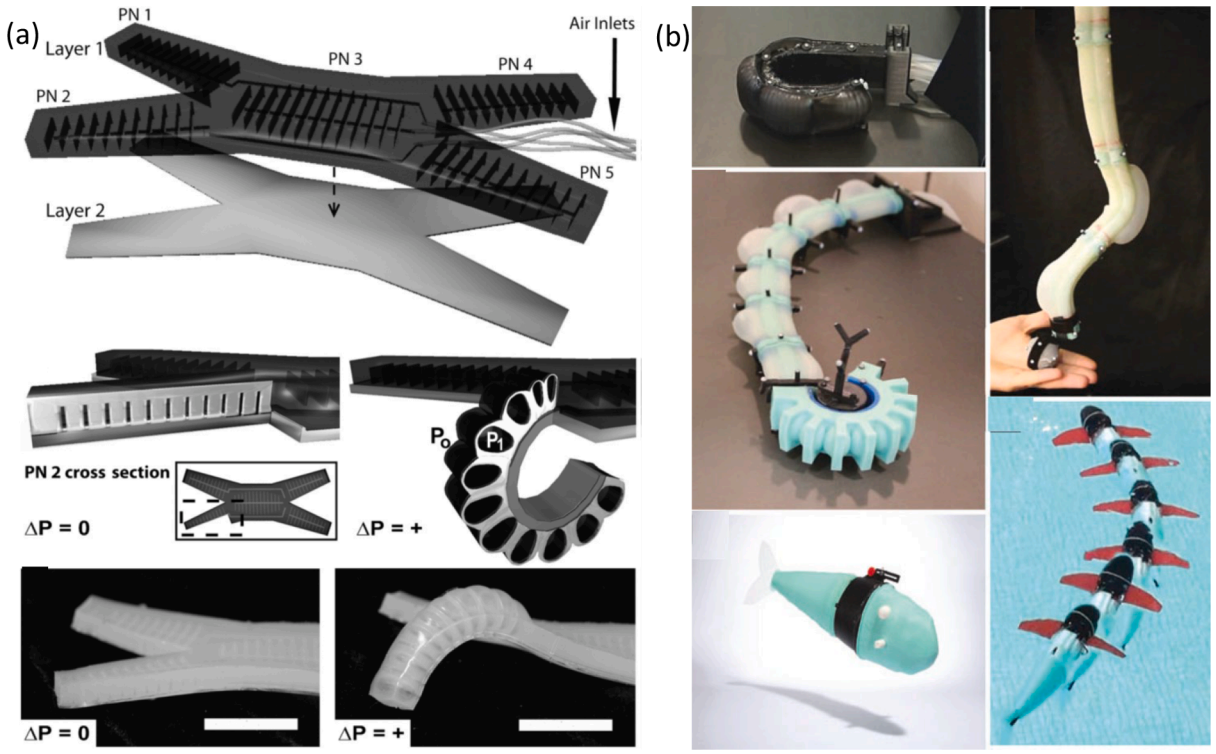

Fig. 4. (a) A schematic representation of the Pneu-net (PN) channels. A series of PN chambers are embedded in an elastomeric layer and bonded to an inextensible layer. When the chambers are pressurized, the difference in the strains causes the structure to bend (Shepherd et al. 2011)[46]. (b) Extremely soft and highly compliant fluidic elastomer robots. Planar, cylindrical manipulators, and self-contained pneumatic and hydraulic fish (Marchese et al. 2015)[47].

Table 1
A list of state-of-the-art technologies for indwelling robot locomotion.

Locomotion	Remarks	Volume/Weight	Velocity	Reference
Burrowing	0.27 J/cm up to 70 cm digging depth	~45 cm^3	-	Nordstrom et al. [33]
Burrowing	The achieved rotation rate of 2 deg/s	~211 cm^3	2 mm/s	Russell R.A. [35]
Crawling	Origami structure accounts for only 8.7% of the whole weight.	220 g	12.3 mm/s	Fang et al. [42]
Crawling	Critical stroke for 15 mm diameter and 20 mm long segments is 7 mm	1.87 cm^3	-	Kwon et al. [43]
Inchworm crawling	A turn rate of 0.71 deg/s is achieved.	54.2 g/DDSM	4.81 mm/s	Wang et al. [46]
Earthworm crawling	Solenoid actuator stroke 15 mm and 5 segments achieve 2deg/s	50 g/segment	27.2 mm/s	Song et al. [44]
Earthworm crawling	Overall length is between 220 mm and 300 mm	380 g	10 mm/s	Omori et al. [41]
Crawling through intestine	Power for locomotion is 0.29 W and 0.405 W including communication.	32 g	0.22 mm/s	Wang et al. [45]
Spider crawling, climbing	Overall diameter 105 mm and working voltage 7.4 V	350 g	~0.16 m/s	Yanagida et al. [47]
Starfish crawling, creeping	The average value of the moving step is 50.7 mm on the sand.	145 g	2.17 mm/s	Mao et al. [48]
Soft crawling robot	Pneumatic tethered actuation up to 3 kg	43 g	6.67 mm/s	Qin et al. [56]
Swimming soft fish	35 minutes of continuous operation over 1.3 Ah Li Polymer battery.	1.65 kg & 0.45 m x 0.19 m x 0.13 m	80 mm/s	Katzschmann et al. [57]
Manta ray swimming	The pneumatic actuator at 0.15 MPa in soft rubber tube of length 70 mm.	170 mm x 150 mm x 10 mm	100 mm/s	Suzumori et al. [58]
Insect inspired walking	A floating speed of 7.14 mm/s and turning speed of 9 deg/s are demonstrated	70 mm x 30 mm x 17 mm	3.6 mm/s	Shi et al. [59]
Octopus inspired soft robot	Soft Octobot is actuated by monopropellant catalytic decomposition.	~ 70 mm x 70 mm x 30 mm	-	Wehner et al. [60]
Paddling based capsule	Wired capsule paddles through the colon in an anesthetized pig over 40 cm	Ø 15 mm x 43 mm	0.28 mm/s	Kim et a. [61]
Spiral wire swimming	Peak velocity occurs with gravity compensation at 14 Hz magnetic fields from 0.7 A.	Ø 6 mm x 60 mm & 1.39 g	36.5 mm/s	Guo et al. [62]
Reel mechanism-based colonoscope	External reel controller with silicone legs for colon safety.	Ø 16 mm x 49 mm	9.55 mm/s	Lee et al. [63]
Propeller enabled locomotion	Peak propulsion force of 25.5 mN with 13 min lifetime.	Ø 22 mm x 32 mm	150 mm/s	De Falco et al. [64]

glycerin compared with water. The propulsion of the swimmers is attributed to the bending oscillation of the tail fin. It is experimentally verified that the microrobot could move through the aortas, veins, and the *vena cavae*. However, motion through smaller arteries, capillaries would require miniaturizing the microrobot [68]. A mechanism to resist peristalsis in the GI tract was proposed occupying only 9% of the total volume of a wireless endoscopic capsule [69]. A completely cordless endoscopic capsule integrated with a camera and battery is realized using propeller-based locomotion that can provide a thrust force of 25.5 mN [64]. To control the capsule in real-time, a frame rate of 23 fps was sufficient using an onboard camera that generated images up to 50 mm of the focal distance. An indwelling ruminal robot is expected to move through the liquid region and regions with varying particle sizes in the rumen. Unlike the tethered endoscopic capsules, the ruminal robot has to be equipped with an independent locomotion mechanism that offers a superior advantage for navigating through both stratified semi-solid and liquid media. A bioinspired flexible soft robotic body with peristaltic and/or multi-segment propeller-based structures combined with vision-based navigation are the potential future directions for implementing locomotion and navigation in indwelling ruminal robots. The state-of-the-art innovations in the localization of the rumen robot are discussed in the next section.

Localization of Rumen Robot

Indwelling biorobots need to navigate in complex and confined spaces inside the body. The data that they collect needs to be correlated with precise locations inside the body for it to hold significance for the users. Hence, the precise localization of such robots is critical. In the case of the rumen, the highly stratified 184-liter volume of gas, coarse and fine matter, and acidic liquid can only be understood if we are able to correlate the sensor measurements with the location. Identification of key areas in the rumen will build a better understanding of its functioning, leading to better prediction models for feed, methane expulsion, and productivity. However, it is an arduous task unlike any other. The rumen is an organ covered in layers of tissues such as bones, muscles, and fat. This attenuates radio frequency signals considerably. Further, there is an inherent power constraint on the device as it needs to stay in the rumen for long durations and cannot be easily extracted for replacing or charging batteries frequently. The rumen is also the largest organ in the body of the cow and is constantly being intermixed with natural contractions. This spatial vastness coupled with the strong opposing forces of the contractions presents a major challenge for any robot not only for localization but also for locomotion. While the prior art in this area is almost non-existent, there is a similar environment that has been thoroughly investigated: the human gastrointestinal (GI) tract.

The Human GI tract is also a dark, acidic, and constantly moving environment that needs wireless robots for mapping. The Human GI tract is mapped using wireless capsule endoscopes (WCE) to detect conditions such as colorectal cancer and polyps. The position and orientation of the WCE as it passes through the GI tract are vital to performing therapeutic operations. Hence, accurate, and precise knowledge of the WCE localization is an inevitable requirement. While numerous technologies developed for robots in human bodies have reached maturity, they are not directly portable to animal applications. The human stomach is not only $1/45^{th}$ (2-4 liters) in size of the rumen; it is covered with a comparatively thin layer of tissues. Since WCEs are not implanted in the GI tract for long durations, they do not face a major power constraint. Further, the human GI tract contains particles of smaller size, whereas the rumen contains a variety of particle sizes floating in a highly acidic fluid. Also, the wireless capsules move along the direction of contraction of the tract, thus saving power and effort. Hence, the need is to investigate and identify methods that can potentially be extrapolated for use in indwelling robots in animals, albeit with significant technological alterations.

In recent years, comprehensive surveys and reviews have been published for technologies used in the localization of WCEs [70,71]. However, in this section, we review these techniques from the perspective of in-rumen localization. There are three primary methods of localizing WCEs: radio frequency, magnetic fields, and image-based localization. Table 2 lists different technologies of localization, with their specifications, discussed in this review.

RF-based localization

WCEs often contain a radio-frequency (RF) module that transmits images and sensor data to a receiver outside the body. This RF signal is also be used localize the WCEs by triangulation based on the characteristics of the received signal with respect to the one that was transmitted. The transceivers are calibrated to the global coordinates, which then translate the local position to global position. RF-based localization (Fig. 5 (a)) is one of the least power-consuming methodologies for the localization of WCEs. They can work with inexpensive hardware that is easy to fabricate. Primarily, three main approaches for localization using RF signal include using the received signal strength indication (RSSI), the Time of Arrival (ToA), and Direction-of-Arrival (DoA). Since RSSI methods are the simplest to implement, they are widely used [76,100].

Using the maximum likelihood algorithm, the 3D location of a WCE traveling in a simulated small intestine (volume of 400 × 200 × 350 mm3) was estimated with an error of 80-110mm in 95% of the cases. The Cramer Rao Lower Bound (CRLB) was used to determine the position errors. Notably, the large distribution of the positional accuracy was attributed to the dependence of WCE on the receiving antenna distance. However, in the case of 3D estimations, from the studies conducted by Ye et al. [73,74] it was found that an arrangement of 32 sensors with a dimensional range of 266 × 323 × 312 mm3 is required to obtain an estimate with an RMSE in the 45-50 mm range. This limitation of low accuracy is one of the biggest impediments in the wide-scale real-life application of RF-based localization.

Time-of-Arrival (ToA) methods estimate position based on the time taken by the signal to reach the receiver from the transmitter, whereas Direction-of-Arrival (DoA) base localization estimates on the direction of the received signal perceived by a set of receiving antenna array. A comprehensive comparative analysis on ToA and RSSI methods concluded that ToA methods are more accurate with error in millimeters whereas for RSSI they were in the centimeters range [76]. Subsequent studies showed that it was possible to obtain error estimates lower than 15 mm through the ToA method [73–75]. Moreover, this error could further be reduced by adding an IMU sensor as described in Fig. 5 (b). In this study, by using an extended Kalman filter with a circular array of antennas to implement both ToA and DoA localization, errors lower than 10 mm and 0.5 cm/s for velocity measurements were achieved by adding an IMU. A localization system with high accuracy using an array of body surface-mounted sensors is shown in Fig. 5 (c) [101]. A similar study showed errors less than 10mm with a set-up that used an unscented Kalman filter along with DoA based localization for a WCE in a patient [78]. A recent study investigated the list of ToA/DOA methods coupled with IMU sensors for localization, illustrating that RMSE lower than 1mm was possible [79]. Hence, these studies proved the efficacy of ToA and DoA localization over RSSI for human WCE applications. However, the implementation of ToA and DoA localization is complicated requiring expensive and unwieldy hardware such as synchronization systems and a set of antenna patterns [102]. Moreover, RF-based methods are unsuitable for rumen applications as they suffer from signal attenuation due to the various layers of tissues, organs, and bones, and frequency-dependent path loss. Also, the size of the receiver array setup needed would be unpractical for the application.

Magnetic localization

Magnetic field strength detection is another popular method for the localization of WCEs. The benefits of using magnetic field-based

Table 2
A summary of the state-of-the-art technologies for localization.

Localization Principle	System Components	Degrees of Freedom	Test Setup	Accuracy	Reference
RF Signal Strength (RSSI)	WCE with RF transmitter and antenna; 4 receiver antennas on body	P: 3D	Simulation ($400 \times 200 \times 350mm^3$)	P: 80-110mm	Li et al. [72]
RF Signal Strength (RSSI)	WCE with RF transmitter and antenna; 32 receiver antennas on body	P:3D	Simulation ($263 \times 323 \times 312mm^3$)	P:45-50mm	Ye et al. [73, 74]
ToA (Time of Arrival)	Transmitter antenna on WCE; 3D array of receiver antenna on body	P:3D	Simulations ($596.9 \times 21.59 \times 203.2$ mm3)	-	Liu et al. [75]
RSSI vs ToA	FDTD simulation in MATLAB	P:3D	Simulation	ToA=3.5cm RSSI = 5.1cm	Khan et al. [76]
ToA (Time of Arrival) and DOA (Direction of Arrival)	WCE with RF transmitter and IM; RF receiver array on the body	P:3D	Simulation	P:10mm	Nafchi et al. [77]
DoA (Direction of Arrival)	WCE with transmitter and IMU; 8 columns of receiver array in room	P: 3D	Simulation in roomspace (10mx5mx2.5m)	P: 2.25 cm (no refraction); P:8cm (with refraction)	Goh et al. [78]
ToA (Time of Arrival) and DOA (Direction of Arrival)	WCE with transmitter and IMU; receiver array outside	P:3D	Simulation ($400 \times 400 \times 400mm^3$)	P:0.5mm (10 sensor, -16dBm path loss)	Jeong et al. [79]
IPM Magnetic Field Sensing	Circular IPM and 16 3-axis Hall effect sensor arrays	P: 3D; O: 2D (pitch/yaw)	Simulation and free space validation	P: 5.6mm; O: 4.26% unit orientation vector	Hu et al. [80]
IPM Magnetic Field Sensing	Circular IPM and 16 3-axis Hall effect sensor arrays	P: 3D; O: 2D (pitch/yaw)	Simulation and free space validation	P: 5.6 mm; O: 4.26% unit orientation vector	Hu et al. [81]
IPM Magnetic Field Sensing	Circular IPM and 16 3-axis Magneto-resistive sensor arrays	P: 3D; O: 2D (pitch/yaw)	Simulation and free space validation	P: 3.3 mm; O: 4.5°	Wang et al. [82]
IPM Magnetic Field Sensing	Circular IPM and 16 3-axis Hall effect sensor arrays	P: 3D; O: 2D (pitch/yaw)	Simulations and free-space validation (240×240 mm^2)	P: 2 mm; O: 1.6°	Hu et al. [83]
IPM Magnetic Field Sensing	Rectangular IPM and 16 3-axis magneto-resistive sensor arrays	P: 3D; O: 3D	Simulations	PA: 3.9 mm* and 0.59 mm**; OA: 5.06°* and 0.66°**	Yang et al. [84]
IPM Magnetic Field Sensing	Rectangular IPM and Cubic array of 64 HMC1043 3-axis sensors	P: 3D; O: 3D	Simulations and Free space validation with a max distance of 250mm between the sensor and capsule	P: 1.82 mm; O: 1.62°	Hu et al. [85]
IPM Magnetic Field Sensing	Annular IPM with cubic magnetic array of 3-axis HMC1043 sensors	P: 3D; O: 3D	Simulation (Volume = $360 \times 370 \times 300m^3$)	P: 0.003 mm; O: 0.036°	Song et al. [86]
IPM Magnetic Field Sensing for wearable application	Ring-shape IPM; a wearable magnetic array of sensors of 32 3-axis magnetic sensors	P: 3D; O: 3D	Simulation and free space validation	P: 3.82 mm; O: 2.2°	Hu et al. [87]
Magnetic Field Sensing for wearable application	16 digital magnetic sensors (LMS303D) and two noise cancellation sensors	P: 3D; O: 3D	Free space validation ($380 \times 270 \times 240$mm)	P: 10mm; O:12°	Shao et al. [88]
External magnetic field and On-board sensing	Sub-miniature induction coil embedded in capsule; 8×8 circular coplanar transmitting coils	P: 3D; O: 3D	Free-space validation (200 mm distance between the coaxial receiving and transmitting coils)	P: 0.75 mm; O: 0.6°	Plotkin et al. [89,90]
External magnetic field and On-board sensing	Internal coil (secondary) used for FM signal generation; 5 alternating magnetic fields generated outside from solenoid coils (primary)	P: 3D; O: 3D	Free-space validation (up to 500 mm to the magnetic field generator)	P: 2.8 ± 2.2 mm; O: 13.4°± 20.9°	Nagaoka and Uchiyama [91]
External magnetic field and On-board sensing	3-orthogonal rectangular coils inside a capsule and used as a tri-axial sensor	P: 3D; O: 3D	Free-space validation (up to 257 mm to the magnetic field generator)	P: 6 ± 0.28 mm; O: 1.11° ± 0.04°	Islam and Fleming [92]
EPM magnetic field Sensing	6-DoFs robotic arm with an EPM; capsule device with IPMs; embedded Hall-effect sensors; 3-axis accelerometer	P: 3D; O: 3D	Free-space validation ($200 \times 200 \times$ 60-120 mm3)	P: 6.2 ± 4.4 mm radial; 6.9 ± 3.9 mm axial; 5.4° ± 7.9° azimuth; O: 0.27° ± 0.17° pitch; 0.34° ± 0.18° yaw; 1.8° ± 1.1° roll	Di Natali et al. [93]
Integrated Camera	WCE with integrated camera	P:3D	Analysis/classification of acquired images using VQ+PCA, ANN and VQ	-	Duda et al. [94]
Integrated Camera	WCE with integrated camera	P:3D	Region-based K-SVM	-	Bao et al. [95]
Integrated Camera	WCE with integrated camera	P:3D	Polyps detection using CNN	-	Brando et al. [96]
Integrated Camera	WCE with integrated camera	P:3D, O:3D	Consecutives frame evaluation	O: 0.3	

(*continued on next page*)

Table 2 (*continued*)

Localization Principle	System Components	Degrees of Freedom	Test Setup	Accuracy	Reference
					Aghanouri et al. [97]
Integrated Camera	WCE with integrated camera; geometric visual odometry based recognition	P:3D	In-vitro experimentation	P: 1.6 ± 1.7cm	Iakovidis et al. [98]
Integrated Camera	WCE with integrated camera; ANN based recognition	P:3D	In-vitro experimentation	P:0.79±0.51cm	Dimas et al. [99]

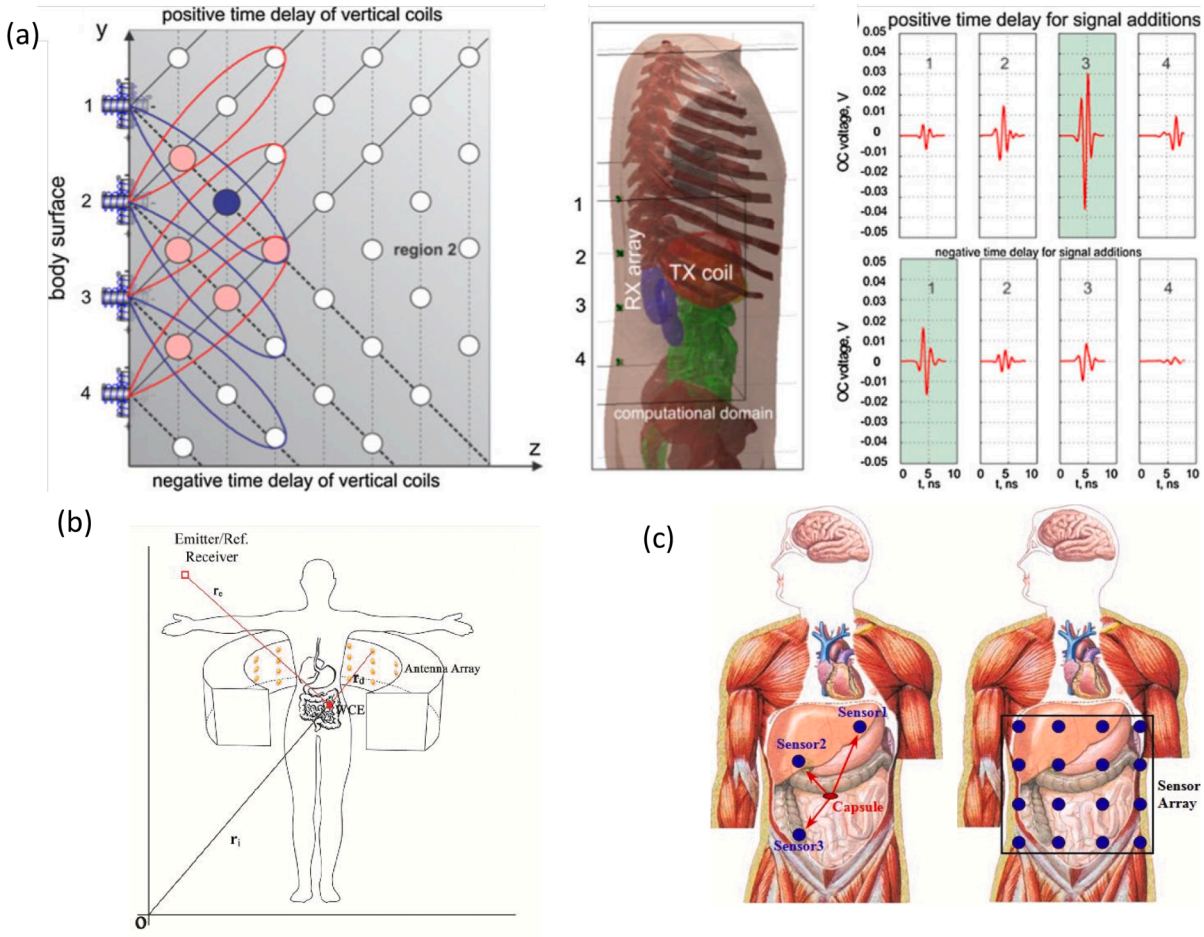

Fig. 5. (a) An array of orthogonal coil antenna to improve the received signal strength [100]. (b) Localization of WCE using circular arrays and inertial measurement unit for ToA and DoA approaches [77]. (c) Two configurations of surface mounted sensors for localization of the capsule [101].

localization include very little attenuation of low-frequency magnetic signals when passing through tissues and directivity independent tracking [103]. Magnetic localization systems can be categorized into two main groups depending upon the placement of the magnetic and the sensing system: first, the magnet on the WCE and the sensing system is outside the body (Fig. 6 (a)) [83,85–87,104,105], and second, magnetic sensors inside the capsule with the magnetic source outside the body [89,90,106]. The use of sensing technology outside with a magnet in WCE was the initial approach in adopting magnetic localization. Using internal permanent magnets (IPM) with an array of hall effect sensors on the outside, maximum accuracy of 5.6mm in position and 4.2% in orientation was achieved, however, the 1.2 second step calculation time fairly limited its application [105]. Consequently, using a linearization of the Levenberg-Marquardt algorithm, this step time was reduced to 10.6ms which is more suitable for such real-time applications [83]. Similarly, tri-axial magnetometers resistive-based sensors yielded better results with an average estimated error of 3.3 mm in case of position and 3° in case of orientation [82].

However, these localization methodologies use optimizers to reduce computation load. While linear optimizers are faster, non-linear optimizers result in better accuracies. Hence, the approach of using a coarse estimate by using the linear optimizer first, and then using the non-linear optimizer to refine the estimate was adopted by Hu et al. [81,83]. They managed to reduce the estimation error to 2 mm and 1.6° for position and orientation, respectively. Moreover, combining an IPM setup of 16 magneto-resistive sensors with Particle Swarm Optimization (PSO) further improved performance with execution time of 0.17s and error rates of 0.59mm mm and 0.666° in position and orientation, respectively [84]. Nevertheless, in order to increase the maximum operating range beyond the previously achieved 120 mm, Hu et al. [85], used a cube-shaped magnetic sensor array composed of 64 tri-axial magnetic sensors to implement real-time tracking of the magnetic field

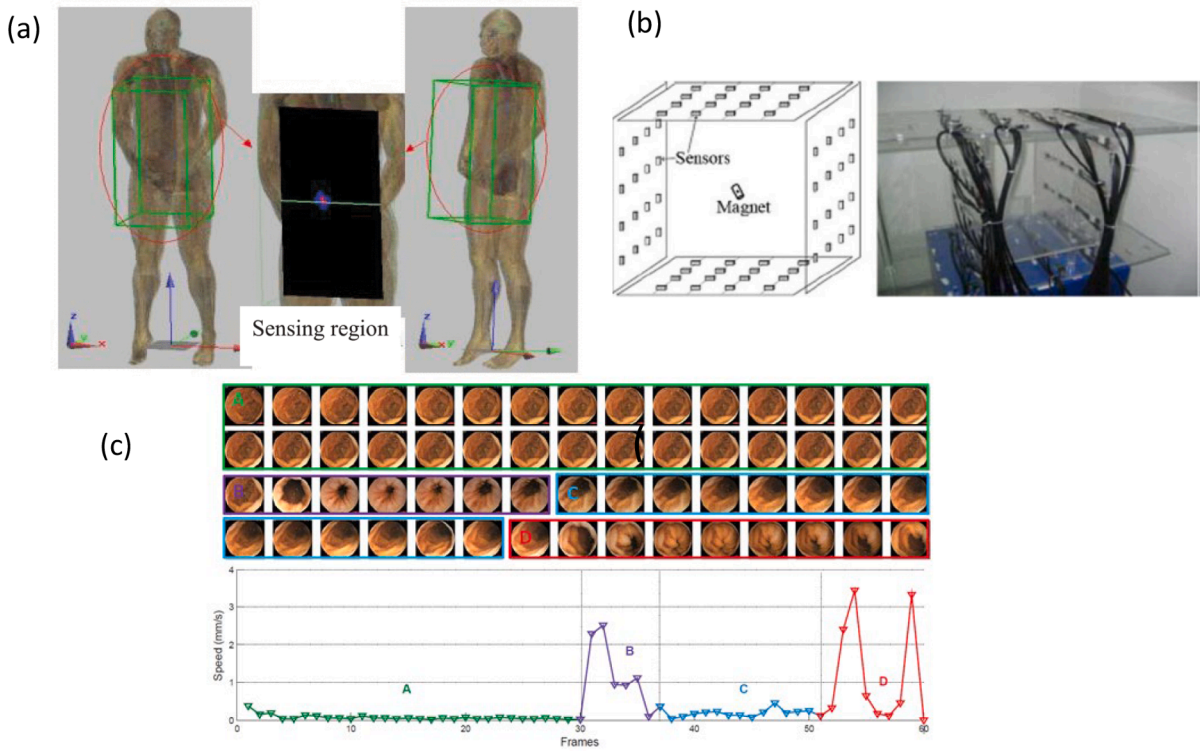

Fig. 6. (a) Tissue absorption-based identification of the location of GI tract in human body [107]. (b) A schematic of the magnetic sensor array and experimental setup. There are 16 magnetic sensors installed on a given plane in a fixed uniform interval [87]. (c) Statistical estimation of speed using the clinical video data [105].

of the IPM as shown in Fig. 6 (b). They reported an average estimation error of 1.82 mm in position with a 1.62° orientation error with a maximum distance of 250 mm between the sensors and the magnet. Replacing rectangular magnets with annular ones (with a radial magnetization direction) resulted in improved performance with an average position error estimate of 0.003 mm and an average orientation error of 0.036°.

While these methods achieved high accuracy, they do not perform well with the motion of the body. Yet, for rumen-dwelling applications, the need is for a wearable system able to compensate for body motion. Recent works using two permanent magnets, one in capsule and one on the body, and a 32 sensor array was able to overcome interferences due to the motion of the body [87]. Similarly, another wearable method that used geo-noise cancellation sensors was proposed which achieved a position error of 10mm and an average orientation error of 12 ° in a volume of 380 mm x 270 mm x 240 mm [88].

In the case of a magnetic source outside with the sensor inside the body, the initial work was presented by Plotkin et al. [89]. They used a single sub-miniature circular induction coil sensor and an 8 × 8 array of circular coplanar transmitting coils which generated magnetic fields that were detected by the single sensing element inside the capsule. Their method resulted in an accuracy of 0.75 mm in position and 0.6 ° in orientation, with a maximum operating range of 200 mm in height above the transmitting array. Similarly, a setup using five alternating external magnetic field sources and a single-axis coil (6.5 mm in diameter, 2.3 mm in height, and 160 turn copper wire) as a sensor was able to localize with an error of 2.8 ± 2.2 mm and 13.4 ± 20.9 ° within a maximum distance of 400 mm [91]. However, the shape of the coils resulted in a considerably bulky structure. Nevertheless, orthogonal rectangular coils, made of 0.08 mm diameter copper wire, enclosed into a wireless capsule of 26 mm in length and 11 mm in diameter were used to solve this tradeoff between size and accuracy [106]. They achieved an estimated error of 6 ± 0.28 mm in position and an error of 1.11 ± 0.04 ° in orientation. Yet, this method is unfeasible for rumen-dwelling robots as the size of the coils needed would be significantly large, making them extremely expensive and impractical.

In addition to these two approaches, another method of detecting the 6D pose of a WCE based on an iterative Jacobian methodology was proposed by Di Natali et al. [93]. They defined a closed-form expression for the Jacobian of the WCE which they then utilized to obtain an iterative localization of the WCE at a faster computational time. They used an Inertial Measurement Unit (IMU), a permanent magnet, and 6 magnetic field sensors. The magnetic field and pose are acquired from the sensors. A digital Kalman filter is implemented on this data which is then sent to the Jacobian-iterative algorithm which in turn returns the 6D capsule pose estimates. The average localization error in cylindrical coordinates was 6.2 ± 4.4 mm and 6.9 ± 3.9 mm in the radial and axial components. This approach is truly useful as there is no external setup required which can allow for easier use, especially in the case of animals.

Image-based localization

Apart from magnetic sensors-based localization, video-based techniques are also being adopted to determine the position and location of a WCE. A method based on computer vision can estimate the capsule speed based on the consecutive frames. Average accuracy of 93% with a localization accuracy of less than 2.49 cm was achieved when applied on the real endoscopic images as shown in Fig. 6 (c) [107]. Pahlavan et al. [93,108] described a cyber-physical system (CPS) architecture, which utilizes 2D pictures taken by the WCE to create a 3D image of the interior of the small intestine as shown in Fig. 7. In this architecture, they postulated that using a Body-SLAM algorithm with their hybrid RF model, their system could attain a precision of 1-2 mm. Identifying GI pathologies and capsule pose estimation was performed by surgeons in initial implementations of visual localization. However, the use of artificial intelligence in the form of deep learning models is steadily gaining preference in such tasks. In a comparative analysis among Vector Quantization (VQ), Artificial Neural Networks (ANN), and VQ + Principal Component Analysis (PCA), it was found that the approach ANN outperformed the rest by reaching 85% success in the

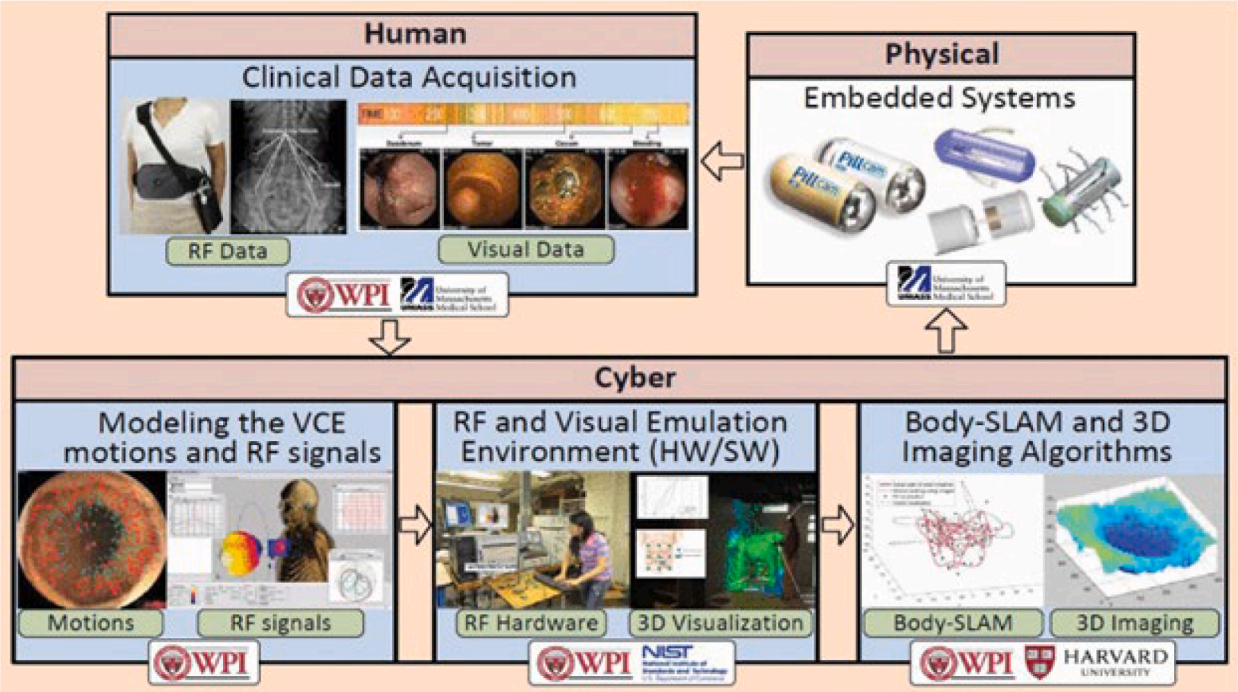

Fig. 7. A cyber physical systems (CPS) architecture utilizing 2D pictures taken by the wireless capsule endoscope (WCE) to create a 3D image of the interior of the small intestine [100].

recognition of features in the GI tract [94]. Similarly, in a comparative analysis of ANN and a region-based kernel support vector machine (K-SVM), the K-SVM classifier outperformed ANN with a recognition percentage of 80-90% in identifying subregions [109]. Convolutional neural networks, due to their incredible performance in image data, have also been tested in use for WCEs. They were used to identify and segment polyps in colonoscopy images with a 93.3% success rate [96]. To estimate the angle of rotation and the distance of the capsule from the stomach wall features extracted using the Speeded Up Robust Features (SURF) method were fed to a model with Fast Library for Approximate nearest neighbors (FLANN) and the M-estimator Sample and Consensus (MSAC) method were used by Aghanouri et al. [110]. Their orientation errors were lower than 0.3 °. In a similar approach, instead of SURF features, Scale Invariant Feature Transformations (SIFT) were used to estimate the distance traveled by the WCE [98]. In this study, they validated the use of in-vitro experiments using video sequences from the public domain. This study was further extended by Dimas et al. [99] in which they used a multilayer feed-forward neural network (MFNN) for estimating the distance covered by the WCE over the axis parallel to the GI lumen for the estimation of the scaling factor. The mean absolute error obtained was 0.79 ± 0.51 cm for a distance of 19.6 cm.

While image-based methods are easier to implement and do not need much in terms of specialized supporting and sensing hardware, they do require a light source and identifiable features, which are not easily available in large organs of animals. Further, they also constrain the lifetime of the capsule as the camera, light source and transmission of the collected data take considerable battery resources. The power and communication constraints limit the application of triangulation and visual localization methods. Also, such methods usually rely on large datasets which are fairly lacking for animals.

In conclusion, after analyzing these three main techniques of localization in the Human GI tract from the perspective of in-rumen applications, we note that RF-based methods are unsuitable for in-rumen applications due to signal attenuation and the large size of the antenna arrays required. Further, image-based localization needs integrated cameras with proper illumination to identify key features. Such key features are not easily identifiable in the large volume of the rumen. Also, there is a paucity of data mapping such features in the rumen. Hence, image/video-based methods also prove to be unsuitable for the application. While magnetic localization techniques can be a potential solution, but they need to be scalable and account for the animal's bodily movements to improve precision in the derived estimates. Hence, we recommend an approach with wearable magnets sensors, that can compensate for movement using an IMU and the jacobian of the robot.

Wireless data transmission

Moving critical data around the human body and outside the body to remote data receivers has been a goal of researchers and medical device manufacturers for decades. Although the transition to animal bodies is obvious, there is very little published work on body sensor networks other than for human applications. Still, the challenges for wireless data transmission from an indwelling device present in a rumen environment inside the animal body to a device out of the body are similar to those encountered in human beings. Low power methods for communication in size-constrained devices are essential in improving battery life span which has been one of the major bottlenecks in human-implantable device technologies [111,112]. The field is broken into two major approaches: "around the body" methods and "through the body" methods. Around the body communication technologies typically use radio frequency (RF) based wireless communication methodologies. These communication paradigms operate at high frequency (~GHz) bands with energy efficiency ranging from hundreds of pJ/bit to well over tens of nJ/bit [113].

Bluetooth-based implantable devices [114] are popular in the medical community for continuous monitoring of patients [115,116]. Commercial devices like insulin pumps, pacemakers, and other cardiac devices have been using Bluetooth for data transmission for quite some time [117]. Bluetooth works at a frequency band of 2.4 GHz and devices operating on Bluetooth can work for a range of about 50 meters [118]. The energy efficiency for Bluetooth-based devices is in the order of 10 nJ/bit. Bluetooth works well as a short-range efficient means of communication but is power-hungry thus affecting the battery life of the device.

The Federal Communications Commission (FCC), the regulatory body for monitoring and establishing protocols for electronic communication around the USA, defined a MedRadio band [119] around the 400 MHz range for implantable devices and devices are worn around the body. The 400 MHz spectrum is a more energy-efficient alternative to Bluetooth with an energy efficiency of less than 1 nJ/bit. Implantable devices working at 400 MHz have also been developed previously for around-the-body applications. Interestingly, this same frequency band is used in one of the few animal-centric papers to determine the electromagnetic attenuation properties of a calf using RFID [120].

The use of LoRa [121–123] technology has also come up as a viable alternative to Bluetooth. The LoRa protocol, as the name suggests, is a long-range communication technology based upon spread spectrum modulation techniques with a range of about 10 kilometers. LoRa is operated in the frequency range of 900 MHz in the USA. The Zigbee protocol [124] has also been used in medical devices for data collection. While suitable for the on-body hub to a long-range gateway, due to the high power and energy need, LoRa is not suitable for intra-body communication. ZigBee is a short-range low power communication protocol working for a range of up to 100 meters depending on the transmission power. ZigBee modules work in the frequency band of 2.4 GHz globally or in the 900 MHz band in the USA.

The above-mentioned RF-based communication technologies work in a frequency range of hundreds of MHz to a few GHz. Such high-frequency communication paradigms are energy inefficient as well as physically insecure. Devices based on Bluetooth are radiative in nature and the transmitted signals are available 5-10 m away from the body. This makes the signal available for attackers with white box or black box knowledge of the system. Ensuring physical layer security of data can add another layer to the security measures present in current WBAN architectures like encryptions. A physically secure system in conjunction with encryption methodologies can further protect data from hackers. To tackle the physical layer security issues as well as to make the communication system less power-hungry, a low-frequency alternative to the RF-based communication technology can be used.

An alternative to the traditional RF-based methods is using the conductive properties of body tissues to transmit the signals at low frequencies of less than 10 MHz. Intrabody communication using the body's conductive properties was first proposed by Zimmerman et al. [125] whereas galvanic Intrabody communication for implantable devices was proposed by Wegmueller et al. [126]. Capacitive Intrabody communication [127] uses a signal plate with a floating ground plate with a direct path to the earth's ground. Due to no direct path being available between the signal plates and the earth's ground for devices implanted into a body, the capacitive modality of intrabody communication cannot be used for implantable device technology. In Galvanic Intrabody communication, a differential signal is passed through two signal plates of the transmitter. The fringe fields pass through the body and are captured at the receiver side attached to the body. Physical layer security [128] is observed in the Electro Quasistatic (EQS) regime where the signal leakage is limited to 5-10 cm around the body. Intra-body communication in the EQS domain also enhances the energy efficiency of the system. The energy efficiency of less than 10 pJ/bit [129, 130] and sub-μW power consumption [131] have been shown for broadband intra-body communication with the frequency of operation in the EQS domain. This gives us orders of magnitude improvement on the energy efficiency and power consumed when compared to popular RF-based methods like Bluetooth and LoRa and hence, this is appropriate for indwelling ruminal robot data communication. A broadband intrabody communication setup in the EQS domain for on-body communication may be used in conjunction with short-range narrowband communication methodologies like Bluetooth and ZigBee for collaborative intelligence [132] around the herd as shown in Fig. 8. This along with long-range communication technologies like LoRa for communication with a central hub has proved to be the most promising framework for wireless data transfer in a sensor network.

Power for indwelling robot

Power and energy sources represent one of the most challenging areas of robotics research and deployment, especially for indwelling robots. The actuators, data communication, and localization elements of a robot can fulfill the intended functions when adequate power is provided. Hence, power management is one of the strictest constraints to

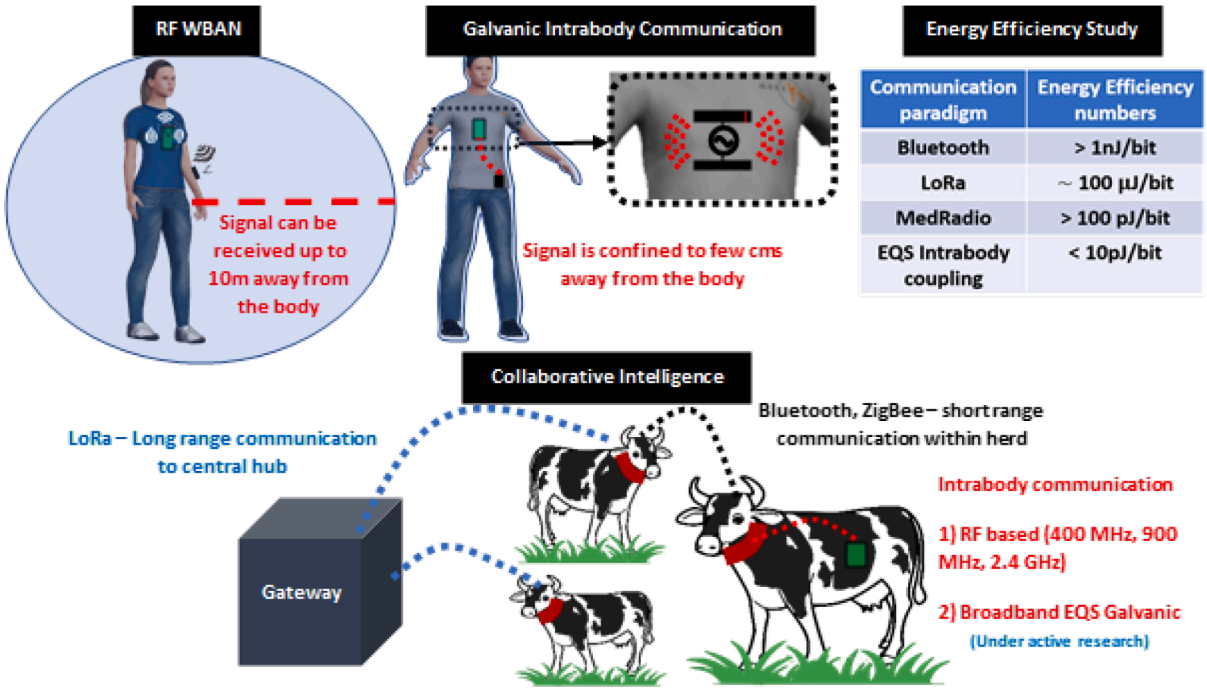

Fig. 8. A comparison between RF based communication methodologies and EQS intrabody communication is shown in terms of physical layer security and energy efficiency. Use of various protocols for collaborative intelligence around a herd environment for energy efficient means of communication is illustrated.

realizing a practical indwelling robot design. The power to an indwelling robot can be supplied in several methods such as the battery, supercapacitor, energy harvesting, magnetic field, and wireless power transfer. Each of the methods is elucidated as follows.

Battery-powered

Batteries offer an inexpensive solution to the power needs of implantable devices. Researchers have even succeeded in implanting a computer in a primate's head with a lithium battery as a power supply [133]. However, because the total deliverable energy scales with volume, batteries are promising power sources for relatively large-scale robots. Although electronic and mechanical systems have been miniaturized by VLSI and MEMS technologies, no counterpart to these exists for electrochemical energy storage. Batteries are often regarded as toxic, which limits their application in animals. Nevertheless, the battery energy densities have almost tripled since 2010 from 0.1 Wh/g to nearly 0.3 Wh/g [134]. The increase in the energy densities has increased the lifespan of batteries in implantable pacemakers to almost 15 years. The adequacy of batteries depends on the indwelling robot functionality, such as locomotion and wireless data transmission, etc. locomotion but also to transmit data wirelessly. Supercapacitors are used in tandem with batteries as the former offers superior power densities juxtaposed with unlimited charge cycles. Apart from the given battery densities, the use of complex neural networking and optimal power management is key to prolonging the lifespan of mobile robots. A concept recharging supercapacitors using ambient energy along with an onboard battery is successfully demonstrated to operate an unmanned ground vehicle with enhanced range of motion [135]. A bottleneck affecting all the commercial capsules is the limited available battery power, providing typically 25 mW for 6–8 h [136]. It is observed that the battery life for implantable pacemakers could be increased to 25 years or more by increasing the volume by about 40%. Recently, practical energy densities of over 0.24 mW/g were achieved by pairing the primary particles of quaternary cathode covered by glassy LiBO2 with Si/C composite anode [137]. Beyond the currently available commercial technologies such as lead-acid, nickel-metal hydride, and lithium-ion batteries, there has been extensive research on developing next-generation technologies, such as fuel cells and stretchable batteries. In light of implementing the peristaltic mechanism in an indwelling robot, flexible batteries are proposed as power sources. The joints in the mechanism could be designed as stretchable batteries decreasing the overall weight and increasing the available volume for sensors and electronics. A rechargeable battery with 1 mAh/cm2 capacity has been realized with stretchability as high as 300% [138]. A 3D printed Li-ion micro-battery is also a viable choice for an indwelling robot. A 3D-interdigitated micro-battery architecture with a high areal energy density of 9.7 J/cm2 at 2.7 mW/cm2 power density within a packaged volume of $<$1mm3 has been successfully realized [139]. Future research in battery power for indwelling robots is focused on using the existing high power density battery architecture as a primary buffer combined with the auxiliary sources in the form of 3D printed battery skin and stretchable joint battery architectures.

Energy harvesting

Energy harvesting is an attractive option to power indwelling robots owing to the non-dependence on depleting energy systems, such as a battery, and the nearly infinite lifetime. The size of the battery often governs the lifetime of the robot. With the use of energy harvesting solutions, the lifetime of the electronic device is increased indefinitely. From using onboard chemical fuels to harvesting vibrational energy from the environment, many such potential solutions have been researched. MEMS-based power generators are of interest because they provide higher energy densities than traditional generators and batteries [140]. The Seebeck effect, in which a temperature gradient develops a voltage differential, makes thermal harvesting another potential option [141,142]. A desirable approach for powering indwelling ruminal robots is to harvest energy from the environment to avoid battery depletion. Numerous devices have been developed for this application, such as piezoelectric polymers and triboelectric nanogenerators [143,144]. M. Han developed a 3D piezoelectric polymer microsystem that can be used for robotic interfaces and biomedical implants [145]. The energy harvesting research on sensors and other biomedical implants [146,147] has to be extended to the indwelling robots with a special focus on the dynamic environment of the rumen. As a result of which, solar harvesting is infeasible, however, microbial fuel cell harvesting is a potential energy harvesting approach. A single sediment microbial fuel cell generating 2.5 mW without the need for a membrane or artificial catalysts has been demonstrated to power a wireless sensor network [148] with a power density of 312 mW/m2. A recent study indicated a maximum power of 13 mW output power from a self-stratifying microbial fuel cell with a specific power of 5.8 mW/g [149]. Alternatively, a dielectric elastomer can be a source of electrical energy when soft body robotics is adopted for the indwelling robot. The repetitive stretching and relaxation of a dielectric elastomer causes a change in the capacitance to a change in the stored electrical energy. Although this is an elementary concept, this principle applied to soft materials is identified as an emerging technology of energy harvesting [150]. At strains less than 15% it is observed that natural rubber outperforms acrylic elastomers and theoretically, energy conversion over 1 J/g is achievable [151]. Mechanical motion is also a suitable energy source for an indwelling robot. The natural contraction and expansion motion of the lungs, heart, and diaphragm has been investigated for energy harvesting in animals. Mechanical-to-electrical energy conversion with high efficiency using advanced materials is required to harvest animal movements. An entire flexible system integrated with rectifiers and micro-batteries capable of harvesting the beating heart motion [152] is demonstrated with efficiencies of ~2%. Although significant levels of electrical power are available for implants, reliable operation of the entire system for the long-term inside the body requires extensive fatigue testing and biocompatibility. Energy harvesting has been used on cardiac implantable devices [153–155], but the requirement for powering implantable robots are much higher than a pacemaker as the power generated from the piezoelectric motion is too low to drive a robot. Hence, efficient energy management of the onboard energy sources is essential to apportion the available energy and discharge the appropriate functions of the robot. Energy harvesting through motion combined with fuel cells and dielectric elastomers are potential areas of research for the power requirements of an indwelling robot.

Magnetic fields driving propulsion

Apart from batteries, a viable option for the actuation and steering of indwelling robots is through magnetic fields. Magnetic fields have a long history of being used to manipulate magnetic devices in the body. A number of wireless power supply systems have been developed for implantable microrobots. Magnetic manipulation has emerged as a promising method in this regard as magnetic fields are capable of penetrating most materials with minimal interaction and are nearly harmless to animals and human beings. Hence, magnetic manipulation is a potential method of powering an indwelling ruminal robot. Magnetic fields have been successfully used to wirelessly manipulate microdevices of various sizes and shapes [156,157]. Magnetic fields and gradients, typically generated from outside the body are used to produce forces and torques on probe masses inside the body. Remote magnetic propulsion can be achieved with magnetic fields and gradients that produce translational forces on the device. Magnetic resonance propulsion (MRP) consists of applying magnetic gradients to exert a displacement force on a ferromagnetic core. The major advantage of this approach is that no complex mechanisms of propulsion need to be integrated onto the microdevice. Instead of building a special platform to

generate such gradients, S. Martel used an MRI system to drive a microrobot into the human blood circulatory system [158–160]. However, for it to be feasible to extend to an indwelling robot, a compact system developed for therapeutic and diagnostic applications [161] using an MRI-Guided nanorobotics system is a suitable approach. S. Chin et al. developed an implantable robot using additive manufacturing and applied it successfully in mice with a rotating magnet of only 1 cm [162]. K. Yesin developed a micro robot using nickel as the magnet and required a magnetic field gradient of 0.7 T/m to drive the 950 × 400 μm elliptical motor in a fluid [163]. Kummer developed a 5-dof motor that is able to puncture retinal veins [156]. O. Ergeneman used a magnetic field to drive a nickel micromotor with a length of only 2 mm [164]. Recent studies on the propulsion of robots have focused on the use of permanent magnets and controlling the movement through the magnetic field from Helmholtz coils [165,166]. Scaling analysis indicates that a large volume of the inserted magnet and the helical flutes offer greater propulsion forces on the robot. Hence, the use of a magnetic field to directly propel the indwelling robot through the rumen is a practicable method of providing motive power to the ruminal robot.

Magnetic fields and wireless power transfer

Magnetic manipulation, in general, is only applicable for limited movement operations, but not for undertaking complicated motion and missions. This is because of the constraints on the input directions of the magnetic field. If propulsion and power can be delivered to the microrobot at the same time, the robot can perform more complex missions over the long term. An alternative approach is to design little or no power storage or generation in the microrobot but instead, wirelessly transmit power to the device. This is achieved using alternating magnetic fields. In this method, time-varying magnetic fields are used to induce currents, creating wireless electricity generation. Additionally, quasi-static and low-frequency magnetic fields are used to apply forces and torques directly to magnetic materials. The body of the cattle is 'transparent' to magnetic fields, which means that the magnetic permeability of the animal body is approximately the same as that of an air vacuum, so there are no significant interactions of tissue with low-frequency magnetic fields as opposed to electric fields.

The basic principle of wirelessly transmitting electrical power with magnetic fields is based on Faraday's law of induction. A schematic of the wireless power transfer concept and the equivalent circuit is shown in Fig. 9. When current is flowing in a circuit (primary), a magnetic field is generated in its surroundings. An effective voltage is developed in any nearby circuit (secondary) proportional to the flux linkage in the secondary coil. The flux density is linearly related to the current in the primary coil. The developed voltage results only from the time-varying component of the primary current, which in practice is sinusoidal, and the geometry that determines the flux crossing the secondary surface. One can increase the induced voltage by increasing the frequency of the primary current or its amplitude, or by modifying the geometry of the circuit arrangement. Increasing the primary current amplitude generates a stronger field, but there is an upper limit on the field strength dictated by safety regulations [167]. Increasing the area of the secondary circuit or bringing it closer to the primary results in an increased flux linkage. Using this concept, a secondary coil can be assembled in the robot while the primary coil stays external to the cow. By transmitting the magnetic fields through the tissues the secondary coil on the robot inside the rumen will harvest the energy wirelessly and charge an onboard battery. Wireless power transfer has been used extensively used for charging electrical vehicles [168] and even drones [169]. Mustafa et al. used wireless transfer to actuate a multi-joint folding robot with a size down to 1 cm x 6 cm [170]. Kim et al. realized a robot that is powered by wireless power transfer to deliver the propulsion force and electrical power simultaneously within a coil size of 110 mm x 100 mm [167]. A design in the form of a tubular shape is often used [171] for wireless power transfer in implantable devices. A wireless power transfer system capable of transferring power as high as 5 W was realized with an efficiency of 88% by Liu et al. [172]. Hence, wireless power transfer is an attractive alternative to meet the power needs and offers huge potential in improving the specific power of the indwelling ruminal

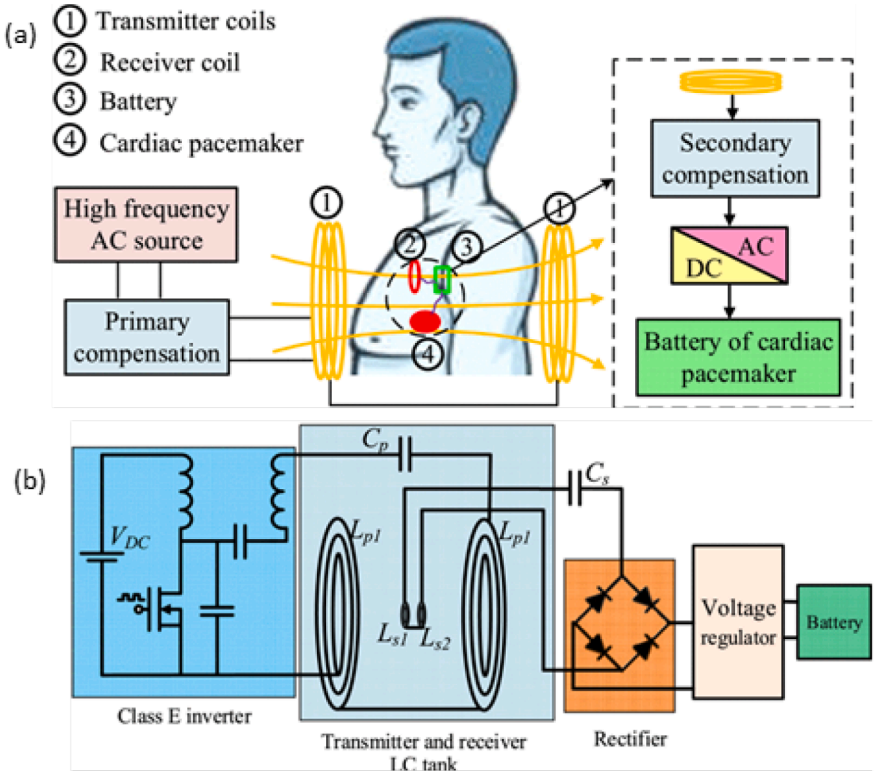

Fig. 9. The concept of wireless power transfer system (a) A sandwiched implantable WPT system and (b) A schematic of the equivalent circuit model [164].

robot by contactless power transfer.

Discussion and future directions

Improving efficiency and productivity of dairy farming is challenge for global food security. Productivity of ruminants is closely tied to their metabolic health which is currently coarsely studied. In this review, we propose the use of a novel indwelling robot for precisely mapping and understanding the rumen dynamics and, to this end, presented state-of-the-art technologies that are essential to design, develop, and implement such an indwelling ruminal robot for health monitoring in cattle. The key elements of a fully functional indwelling robot include locomotion, localization, and wireless data transmission. The navigation, guidance, and control of the robot must be achieved by providing sufficient power to each element. Several approaches of locomotion are discussed listing the key features focusing on weight and volume attributes, achieved velocity levels, and conventional or the nascent soft robotics body. Three significant localization approaches – radio frequency, magnetic field, image-based localization for an indwelling robotic capsule are discussed. Different wireless data communication techniques – RF, MedRadio, LoRa, and EQS regime, are compared in terms of energy efficiency and power consumption. Different methods of providing power to an indwelling robot are discussed with a special focus on energy harvesting and wireless power transfer techniques.

The realization of a fully implantable robot to enhance physiological processes is a grand challenge particularly, a ruminal indwelling robot. Some of the demanding features of indwelling robots include reliability, power autonomy, and biocompatibility. Reliability is the feature of utmost importance as the robot must adapt to the prevailing operating conditions and avert malfunctions. In the case of the rumen, this is even more critical as the size is notably greater and has more complex physiologies. The ruminal fluid constituents motivate a combination of soft robotic and hard robotic locomotion strategies for the indwelling robot. A locomotion technology using soft robotic design to swim through the ruminal liquid and hard robotic design to crawl through the semisolid regions of the rumen pose great challenges. Soft robotics using pneumatic actuation combined with rigid link locomotion are potential methods of navigating a robot through the rumen. The physiological extents of the rumen and the large range of locomotion of ruminal robots impose stringent constraints on the localization precision. The magnetic field-based localization is the most suitable strategy for ruminal robots owing to very little attenuation of low-frequency magnetic fields through tissues. The accuracy of the adopted localization strategy is a crucial metric to navigate and achieve consistent location-based ruminal measurements. An energy-efficient wireless data transmission scheme and data security are critical aspects of the indwelling robots to ensure the privacy and safety of the animal. Low signal leakage and enhanced energy efficiency attract the implementation of the electro quasistatic intrabody communication in the indwelling robot. Power management methodology is imperative for achieving longevity and power autonomy in ruminal robots. High power density energy storage with rational energy apportionment and wireless power transfer energy harvesting strategies impart a long life to the indwelling robot eliminating the need for its removal or battery replacement. The current state-of-the-art technologies and the advancements in locomotion, localization, wireless data, and power transmission have a tremendous impact on the development of an indwelling ruminal robot for animal health monitoring.

Declaration of Competing Interests

The authors declare that they have no known competing financial interests or personal relationships that could have appeared to influence the work reported in this paper.

Acknowledgment

R.S. and X.L. would like to acknowledge the support of the USDA/NIFA through NRI grant # 101339. S.P. would like to acknowledge the support of the USDA/NIFA through CPS grant # 102191, while U.K., X. M., A.D., S.S., and R.V. acknowledge the support of the USDA/NIFA through NRI grant 2019-67021-28990 and through CPS grant 2018-67007-28439.

References

[1] A. McLeod, World Livestock 2011 - Livestock in Food Security, 2011. World livestock 2011 - livestock in food security.
[2] J.M. MacDonald, J. Cessna, R. Mosheim, Changing Structure, Financial Risks, and Government Policy for the US Dairy Industry, US Department of Agriculture, Economic Research Service, 2016. **1477-2017-3966.**
[3] I. Halachmi, H. Levit, V. Bloch, Current Trends and Perspective of Precision Livestock Farming (PLF) with Relation to IoT and Data Science Tools, 2019.
[4] R. Pfeifer, M. Lungarella, F. Iida, Self-organization, embodiment, and biologically inspired robotics, Science 318 (5853) (2007) 1088–1093.
[5] Robotics Society of Southern California [Online], 2022. Available, http://web.cs ulb.edu/~wmartinz/rssc/content/w-grey-walter-and-his-turtle-robots.html.
[6] L.Y. Wang, F. Iida, Deformation in soft-matter robotics a categorization and quantitative characterization, IEEE Robot. Automat. Mag. 22 (3) (2015) 125–139.
[7] D. Trivedi, A. Lotfi, C.D. Rahn, Geometrically exact models for soft robotic manipulators, IEEE Trans. Rob. 24 (4) (2008) 773–780.
[8] D. Trivedi, et al., Soft robotics: biological inspiration, state of the art, and future research, Appl. Bionics Biomech. 5 (2008), 520417.
[9] D. Rus, M.T. Tolley, Design, fabrication and control of soft robots, Nature 521 (7553) (2015) 467–475.
[10] A.D. Marchese, R. Tedrake, D. Rus, Dynamics and trajectory optimization for a soft spatial fluidic elastomer manipulator, Int. J. Rob. Res. 35 (8) (2016) 1000–1019.
[11] K. Suzumori, Elastic materials producing compliant robots, Rob. Autom. Syst. 18 (1-2) (1996) 135–140.
[12] G.Z. Yang, et al., The grand challenges of science robotics, Sci. Robotics 3 (14) (2018).
[13] D.D. Damian, et al., Robotic implant to apply tissue traction forces in the treatment of esophageal atresia, in: 2014 IEEE International Conference on Robotics and Automation (ICRA), IEEE, 2014.
[14] M. Cianchetti, et al., Biomedical applications of soft robotics, Nat. Rev. Mater. 3 (6) (2018) 143–153.
[15] Y.L. Park, et al., Design and control of a bio-inspired soft wearable robotic device for ankle-foot rehabilitation, Bioinspiration Biomimetics 9 (1) (2014).
[16] L. Sonntag, J. Simmchen, V. Magdanz, Nano-and micromotors designed for cancer therapy, Molecules (18) (2019) 24.
[17] B. Wang, Y.B. Zhang, L. Zhang, Recent progress on micro- and nano-robots: towards in vivo tracking and localization, Quantit. Imag. Med. Surg. 8 (5) (2018) 461–479.
[18] D.D. Damian, et al., In vivo tissue regeneration with robotic implants, Sci. Robot. 3 (14) (2018).
[19] C.J. Payne, et al., Soft robotic ventricular assist device with septal bracing for therapy of heart failure, Sci. Robot. 2 (12) (2017).
[20] V. Iacovacci, et al., Design and development of a mechatronic system for noninvasive refilling of implantable artificial pancreas, Ieee-Asme Trans. Mechatron. 20 (3) (2015) 1160–1169.
[21] C.S. Han, et al., Invited review: sensor technologies for real-time monitoring of the rumen environment, J. Dairy Sci. (2022).
[22] C.H. Knight, Review: sensor techniques in ruminants: more than fitness trackers, Animal 14 (2020) s187–s195.
[23] E. Humer, et al., Signals for identifying cows at risk of subacute ruminal acidosis in dairy veterinary practice, J. Anim. Physiol. Anim. Nutr. (Berl.) 102 (2) (2018) 380–392.
[24] H. Dogan, M. Yavuz, A New Wireless Bolus Sensor with Active RFID tag to Measure Rumen pH, 2018.
[25] N. Phillips, et al., Continuous monitoring of ruminal pH using wireless telemetry, Animal Production Science 50 (1) (2009) 72–77.
[26] L. Zhang, et al., Solid-state pH sensor prototype for real-time monitoring of the rumen pH value of Japanese cows, Microsyst. Technol. 24 (1) (2018) 457–463.
[27] C.B. Navarre, A.J. Roussel, Gastrointestinal motility and disease in large animals, J. Vet. Intern. Med. 10 (2) (1996) 51–59.
[28] D.R. Yáñez-Ruiz, L. Abecia, C.J. Newbold, Manipulating rumen microbiome and fermentation through interventions during early life: a review, Front. Microbiol. 6 (1133) (2015).
[29] T. Lyons, et al., Linseed oil supplementation of lambs' diet in early life leads to persistent changes in rumen microbiome structure, Front. Microbiol. 8 (2017) 1656.
[30] R. Danielsson, et al., Methane production in dairy cows correlates with rumen methanogenic and bacterial community structure, Front. Microbiol. 8 (2017) 226.
[31] PubMed-by-Year, 2022. Available, https://esperr.github.io/pubmed-by-year/.
[32] H. Yuk, et al., Shape memory alloy-based small crawling robots inspired by C. elegans, Bioinspiration Biomimetics 6 (4) (2011).

[33] K.N. Nordstrom, et al., Microstructural view of burrowing with a bioinspired digging robot, Phys. Rev. E 92 (4) (2015).
[34] M. Isava, A.G. Winter, Razor clam-inspired burrowing in dry soil, Int. J. Non Linear Mech. 81 (2016) 30–39.
[35] R.A. Russell, CRABOT: A biomimetic burrowing robot designed for underground chemical source location, Adv. Robot. 25 (1-2) (2011) 119–134.
[36] S. Huang, J. Tao, Bio-Inspired Dual-Anchor Burrowing: Effect of Vertical Curvature of the Shell, American Society of Civil Engineers, Reston, VA, 2022.
[37] A. Shukla, H. Karki, Application of robotics in offshore oil and gas industry— A review Part II, Rob. Autom. Syst. 75 (2016) 508–524.
[38] S. Yim, et al., Biopsy using a magnetic capsule endoscope carrying, releasing, and retrieving Untethered Microgrippers, IEEE Trans. Biomed. Eng. 61 (2) (2014) 513–521.
[39] C. Alvarez-Lorenzo, A. Concheiro, Bioinspired drug delivery systems, Curr. Opin. Biotechnol. 24 (6) (2013) 1167–1173.
[40] A. Fukunaga, Earthwormlike exploratory robots, NASA Tech. Brief 22 (1998) 138.
[41] H. Omori, T. Nakamura, T. Yada, An underground explorer robot based on peristaltic crawling of earthworms, Industrial Robot 36 (4) (2009) 358–364.
[42] H. Fang, Y. Zhang, K. Wang, Origami-based earthworm-like locomotion robots, Bioinspiration Biomimetics 12 (6) (2017), 065003.
[43] J. Kwon, et al., Evaluation of the critical stroke of an earthworm-like robot for capsule endoscopes, in: Proceedings of the Institution of Mechanical Engineers, Part H: Journal of Engineering in Medicine 221, 2007, pp. 397–405.
[44] C.-W. Song, D.-J. Lee, S.-Y. Lee, Bioinspired segment robot with earthworm-like plane locomotion, J. Bionic Eng. 13 (2) (2016) 292–302.
[45] K. Wang, et al., An earthworm-like robotic endoscope system for human intestine: design, analysis, and experiment, Ann. Biomed. Eng. 37 (1) (2009) 210–221.
[46] J. Wang, et al., Study on nonlinear crawling locomotion of modular differential drive soft robot, Nonlinear Dyn. 97 (2) (2019) 1107–1123.
[47] T. Yanagida, et al., Design and implementation of a shape shifting rolling–crawling–wall-climbing robot, Appl. Sci. 7 (4) (2017) 342.
[48] S. Mao, et al., Gait study and pattern generation of a starfish-like soft robot with flexible rays actuated by SMAs, J. Bionic Eng. 11 (3) (2014) 400–411.
[49] S. Kim, C. Laschi, B. Trimmer, Soft robotics: a bioinspired evolution in robotics, Trends Biotechnol. 31 (5) (2013) 287–294.
[50] H. Lipson, Challenges and opportunities for design, simulation, and fabrication of soft robots, Soft Robot. 1 (1) (2014) 21–27.
[51] S. Chen, et al., Soft crawling robots: design, actuation, and locomotion, Adv. Mater. Technol. 5 (2) (2020), 1900837.
[52] A.D. Marchese, C.D. Onal, D. Rus, Autonomous soft robotic fish capable of escape maneuvers using fluidic elastomer actuators, Soft Robotics 1 (1) (2014) 75–87.
[53] R.F. Shepherd, et al., Multigait soft robot, in: Proceedings of the National Academy of Sciences of the United States of America 108, 2011, pp. 20400–20403.
[54] A.D. Marchese, R.K. Katzschmann, D. Rus, A recipe for soft fluidic elastomer robots, Soft Robot. 2 (1) (2015) 7–25.
[55] C. Majidi, Soft robotics: a perspective-current trends and prospects for the future, Soft Robot. 1 (1) (2014) 5–11.
[56] L. Qin, et al., A versatile soft crawling robot with rapid locomotion, Soft Robot. 6 (4) (2019) 455–467.
[57] R.K. Katzschmann, A.D. Marchese, D. Rus, Hydraulic autonomous soft robotic fish for 3D swimming. Experimental Robotics, Springer, 2016.
[58] K. Suzumori, et al., A bending pneumatic rubber actuator realizing soft-bodied manta swimming robot, in: Proceedings 2007 IEEE International Conference on Robotics and Automation, IEEE, 2007.
[59] L. Shi, et al., A novel soft biomimetic microrobot with two motion attitudes, Sensors 12 (12) (2012) 16732–16758.
[60] M. Wehner, et al., An integrated design and fabrication strategy for entirely soft, autonomous robots, Nature 536 (7617) (2016) 451–455.
[61] H.M. Kim, et al., Active locomotion of a paddling-based capsule endoscope in an in vitro and in vivo experiment (with videos), Gastrointest. Endosc. 72 (2) (2010) 381–387.
[62] J. Guo, et al., Development of wireless endoscope with symmetrical motion characteristics, Int. J. Adv. Rob. Syst. 11 (9) (2014) 148.
[63] D. Lee, et al., A reel mechanism-based robotic colonoscope with high safety and maneuverability, Surg. Endosc. 33 (1) (2019) 322–332.
[64] I. De Falco, et al., An integrated system for wireless capsule endoscopy in a liquid-distended stomach, IEEE Trans. Biomed. Eng. 61 (3) (2013) 794–804.
[65] T. Honda, K.I. Arai, K. Ishiyama, Micro swimming mechanisms propelled by external magnetic fields, IEEE Trans. Magn. 32 (5) (1996) 5085–5087.
[66] J. Lighthill, Flagellar hydrodynamics - Neumann,Jv Lecture, 1975, SIAM Rev. 18 (2) (1976) 161–230.
[67] S. Sudo, S. Segawa, T. Honda, Magnetic swimming mechanism in a viscous liquid, J. Intell. Mater. Syst. Struct. 17 (8-9) (2006) 729–736.
[68] G. Ciuti, et al., Frontiers of robotic endoscopic capsules: a review, J. Micro-bio Robot. 11 (1-4) (2016) 1–18.
[69] S. Woods, T. Constandinou, Engineering micromechanical systems for the next generation wireless capsule endoscopy, Biomed. Res. Int. 2015 (2015).
[70] G. Ciuti, et al., Frontiers of Robotic Endoscopic Capsules: A Review, Springer Verlag, 2016, pp. 1–18.
[71] N. Dey, et al., Wireless Capsule Gastrointestinal Endoscopy: Direction-of-Arrival Estimation Based Localization Survey, Institute of Electrical and Electronics Engineers, 2017, pp. 2–11.
[72] H. Li, G. Yan, G. Ma, An active endoscopic robot based on wireless power transmission and electromagnetic localization, Int. J. Med. Rob. Comput. Assisted Surg. 4 (4) (2008) 355–367.
[73] Y. Ye, et al., Accuracy of RSS-based RF localization in multi-capsule endoscopy, Int. J. Wireless Inf. Networks 19 (3) (2012) 229–238.
[74] Y. Ye, et al., Comparative performance evaluation of RF localization for wireless capsule endoscopy applications, Int. J. Wireless Inf. Networks 21 (3) (2014) 208–222.
[75] Z. Liu, et al., Wideband characterization of RF propagation for TOA localization of Wireless video Capsule Endoscope inside small intestine, in: IEEE International Symposium on Personal, Indoor and Mobile Radio Communications, PIMRC, 2013.
[76] U.I. Khan, K. Pahlavan, S. Makarov, Comparison of TOA and RSS Based Techniques for RF Localization Inside Human Tissue, 2022.
[77] A.R. Nafchi, S.T. Goh, S.A.R. Zekavat, Circular arrays and inertial measurement unit for DOA/TOA/TDOA-based endoscopy capsule localization: performance and complexity investigation, IEEE Sensors J. 14 (11) (2014) 3791–3799.
[78] S.T. Goh, S.A.R. Zekavat, K. Pahlavan, DOA-based endoscopy capsule localization and orientation estimation via unscented kalman filter, IEEE Sensors J. 14 (11) (2014) 3819–3829.
[79] S. Jeong, et al., Fundamental limits of TOA/DOA and inertial measurement unit-based wireless capsule endoscopy hybrid localization, Int. J. Wireless Inf. Networks 24 (2) (2017) 169–179.
[80] C. Hu, M.Q. Meng, M. Mandal, Efficient Magnetic Localization and Orientation Technique for Capsule Endoscopy, 2022.
[81] C. Hu, M.Q.H. Meng, M. Mandal, Efficient Linear Algorithm for Magnetic Localization and Orientation in Capsule Endoscopy, 2022.
[82] X. Wang, M.Q.H. Meng, C. Hu, A Localization Method Using 3-Axis Magnetoresistive Sensors for Tracking of Capsule Endoscope, 2022.
[83] C. Hu, et al., An Improved Magnetic Localization and Orientation Algorithm for Wireless Capsule Endoscope, 2022.
[84] W. Yang, et al., A six-dimensional magnetic localization algorithm for a rectangular magnet objective based on a particle swarm optimizer, IEEE Trans. Magn. 45 (8) (2009) 3092–3099.
[85] C. Hu, et al., A cubic 3-axis magnetic sensor array for wirelessly tracking magnet position and orientation, IEEE Sensors J. 10 (5) (2010) 903–913.
[86] S. Song, et al., 6-D magnetic localization and orientation method for an annular magnet based on a closed-form analytical model, IEEE Trans. Magn. 50 (9) (2014).
[87] C. Hu, et al., Locating intra-body capsule object by three-magnet sensing system, IEEE Sensors J. 16 (13) (2016) 5167–5176.
[88] G. Shao, et al., A novel passive magnetic localization wearable system for wireless capsule endoscopy, IEEE Sensors J. 19 (9) (2019) 3462–3472.
[89] A. Plotkin, E. Paperno, 3-D magnetic tracking of a single subminiature coil with a large 2-d array of uniaxial transmitters, IEEE Trans. Magn. 39 (5 II) (2003) 3295–3297.
[90] A. Plotkin, et al., A new calibration procedure for magnetic tracking systems, IEEE Trans. Magn. 44 (11 PART 2) (2008) 4525–4528.
[91] T. Nagaoka, A. Uchiyama, Development of a small wireless position sensor for medical capsule devices, in: Annual International Conference of the IEEE Engineering in Medicine and Biology - Proceedings, 2004.
[92] M.N. Islam, A.J. Fleming, A Novel and Compatible Sensing Coil For a Capsule in Wireless Capsule Endoscopy for Real Time Localization, 2022.
[93] C. Di Natali, et al., Jacobian-based iterative method for magnetic localization in robotic capsule endoscopy, IEEE Trans. Rob. 32 (2) (2016) 327–338.
[94] K. Duda, et al., Localization of endoscopic capsule in the GI tract based on MPEG-7 visual descriptors, in: Proceedings of the 2007 IEEE International Workshop on Imaging Systems and Techniques, IST'07, 2007.
[95] G. Bao, K. Pahlavan, L. Mi, Hybrid localization of microrobotic endoscopic capsule inside small intestine by data fusion of vision and RF sensors, IEEE Sensors J. 15 (5) (2015) 2669–2678.
[96] P. Brandao, et al., Fully Convolutional Neural Networks for Polyp Segmentation in Colonoscopy, 2022.
[97] M. Aghanouri, et al., New image-guided method for localisation of an active capsule endoscope in the stomach, IET Image Proc. 13 (12) (2019) 2321–2327.
[98] D.K. Iakovidis, et al., Robotic Validation of Visual Odometry for Wireless Capsule Endoscopy, 2022.
[99] G. Dimas, et al., Visual Localization of Wireless Capsule Endoscopes Aided by Artificial Neural Networks, 2022.
[100] K. Pahlavan, et al., RF localization for wireless video capsule endoscopy, Int. J. Wireless Inf. Networks 19 (4) (2012) 326–340.
[101] M. Pourhomayoun, Z. Jin, M.L. Fowler, Accurate localization of in-body medical implants based on spatial sparsity, IEEE Trans. Biomed. Eng. 61 (2) (2013) 590–597.
[102] F. Bianchi, et al., An innovative robotic platform for magnetically-driven painless colonoscopy, Ann. Transl. Med. 5 (21) (2017).
[103] N.C. Atuegwu, R.L. Galloway, Volumetric characterization of the Aurora magnetic tracker system for image-guided transorbital endoscopic procedures, Phys. Med. Biol. 53 (16) (2008) 4355–4368.
[104] L. Wang, et al., A novel radio propagation radiation model for location of the capsule in GI tract, in: 2009 IEEE International Conference on Robotics and Biomimetics, ROBIO 2009, 2009.
[105] C. Hu, M.Q.H. Meng, M. Mandal, Efficient magnetic localization and orientation technique for capsule endoscopy, Int. J. Inf. Acquisition 2 (1) (2005) 23–36.

[106] M.N. Islam, A.J. Fleming, A novel and compatible sensing coil for a capsule in wireless capsule endoscopy for real time localization, in: Proceedings of IEEE Sensors, 2014.
[107] G. Bao, et al., A video-based speed estimation technique for localizing the wireless capsule endoscope inside gastrointestinal tract, in: 2014 36th Annual International Conference of the IEEE Engineering in Medicine and Biology Society, IEEE, 2014.
[108] K. Pahlavan, et al., A novel cyber physical system for 3-D imaging of the small intestine in vivo, IEEE Access 3 (2015) 2730–2742.
[109] G. Bao, L. Mi, K. Pahlavan, A video aided RF localization technique for the wireless capsule endoscope (WCE) inside small intestine, in: Proceedings of the 8th International Conference on Body Area Networks, BodyNets 2013, 2013.
[110] M. Aghanouri, A. Ghaffari, N. Dadashi, Image-Based Localization of the Active Wireless Capsule Endoscope Inside the Stomach, 2022.
[111] I.F. Akyildiz, et al., Wireless sensor networks: a survey, Comput. Networks 38 (4) (2002) 393–422.
[112] K.C. Barr, K. Asanović, Energy-aware lossless data compression, ACM Trans. Comput. Syst. 24 (3) (2006) 250–291.
[113] S. Sen, Invited: Context-aware energy-efficient communication for IoT sensor nodes, in: 2016 53nd ACM/EDAC/IEEE Design Automation Conference (DAC), 2016.
[114] J. Tosi, et al., Performance evaluation of bluetooth low energy: a systematic review, Sensors 17 (2017) 2898.
[115] K. Weeks, et al., Implantable cathodic voltage controlled electrical stimulator, Electron. Lett 55 (23) (2019) 1215–1217.
[116] T. Wu, J.-M. Redouté, M.R. Yuce, A wireless implantable sensor design with subcutaneous energy harvesting for long-term IoT healthcare applications, IEEE Access 6 (2018) 35801–35808.
[117] Confirm RX™ ICM with Sharpsense™ Technology - Abbott Laboratories, 2022. https://www.cardiovascular.abbott/us/en/hcp/products/cardiac-rhythm-management/confirm-rx-insertable-cardiac-monitor/ht-tab/details.html.
[118] www.bluetooth.com. Understanding Bluetooth Range, 2022 [cited04/30/2022], https://www.bluetooth.com/learn-about-bluetooth/key-attributes/range/.].
[119] FCC Medradio - [online], 2022. https://www.fcc.gov/medical-device-radiocommunications-service-medradio.
[120] H. Dogan, et al., Signal level performance variation of radio frequency identification tags used in cow body, Int. J. RF Microwave Comput. Aided Eng. 29 (7) (2019) e21674.
[121] M. Chiani, A. Elzanaty, On the LoRa modulation for IoT: waveform properties and spectral analysis, IEEE Internet Things J. 6 (5) (2019) 8463–8470.
[122] N. Sornin, et al., Lorawan Specification, LoRa alliance, 2015.
[123] T. Bouguera, et al., Energy consumption model for sensor nodes based on LoRa and LoRaWAN, Sensors 18 (7) (2018) 2104. Basel, Switzerland.
[124] ZigBee Alliance, 2015 [Online]. Available, http://www.zigbee.org.
[125] T.G. Zimmerman, Personal area networks: near-field intrabody communication, IBM Syst. J. 35 (3.4) (1996) 609–617.
[126] M.S. Wegmueller, et al., Signal transmission by galvanic coupling through the human body, IEEE Trans. Instrum. Meas. 59 (4) (2010) 963–969.
[127] S. Maity, et al., Bio-physical modeling, characterization, and optimization of electro-quasistatic human body communication, IEEE Trans. Biomed. Eng. 66 (6) (2019) 1791–1802.
[128] D. Das, et al., Enabling covert body area network using electro-quasistatic human body communication, Sci. Rep. 9 (1) (2019) 4160.
[129] S. Maity, et al., BodyWire: A 6.3-pJ/b 30-Mb/s −30-dB SIR-tolerant broadband interference-robust human body communication transceiver using time domain interference rejection, IEEE J. Solid-State Circuits 54 (10) (2019) 2892–2906.
[130] S. Maity, et al., A 6.3pJ/b 30Mbps −30dB SIR-tolerant broadband interference-robust human body communication transceiver using time domain signal-interference separation, in: 2018 IEEE Custom Integrated Circuits Conference (CICC), 2018.
[131] S. Maity, et al., A 415 nW Physically and Mathematically Secure Electro-Quasistatic HBC Node in 65nm CMOS for Authentication and Medical Applications, in: 2020 IEEE Custom Integrated Circuits Conference (CICC), 2020.
[132] IoTJ submission in ArXiv, B. Chatterjee, et al., Context-Aware Collaborative-Intelligence with Spatio-Temporal In-Sensor-Analytics for Efficient Communication in a Large-Area IoT Testbed, arXiv, 2020, 2005.13003v1 [cs.NI], May.
[133] J. Mavoori, et al., An autonomous implantable computer for neural recording and stimulation in unrestrained primates, J. Neurosci. Methods 148 (1) (2005) 71–77.
[134] BloombergNEF Summit, 2020 [Online]. Available, https://cleantechnica.com/2020/02/19/bloombergnef-lithium-ion-battery-cell-densities-have-almost-tripled-since-2010/.
[135] N. Shah, D. Czarkowski, Supercapacitors in tandem with batteries to prolong the range of ugv systems, Electronics 7 (1) (2018) 6.
[136] P. Swain, The future of wireless capsule endoscopy, World J. Gastroenterol. 14 (26) (2008) 4142–4145.
[137] X. Tang, et al., Towards the high-energy-density battery with broader temperature adaptability: self-discharge mitigation of quaternary nickel-rich cathode, Energy Storage Mater. 33 (2020) 239–249.
[138] S. Xu, et al., Stretchable batteries with self-similar serpentine interconnects and integrated wireless recharging systems, Nat. Commun. 4 (1) (2013) 1–8.
[139] K. Sun, et al., 3D printing of interdigitated Li-Ion microbattery architectures, Adv. Mater. 25 (33) (2013) 4539–4543.
[140] S.A. Jacobson, A.H. Epstein, An informal survey of power MEMS, in: The International Symposium on Micro-Mechanical Engineering, Tsuchiura, Japan, 2003.
[141] F.J. DiSalvo, Thermoelectric cooling and power generation, Science 285 (5428) (1999) 703–706.
[142] S.O. Kasap, Principles of Electronic Materials and Devices, 3 Ed., McGraw-Hill, New York, 2006.
[143] G.-Z. Yang, et al., The grand challenges of science robotics, Sci. Robot. 3 (14) (2018) eaar7650.
[144] Z. Liu, et al., Wearable and implantable triboelectric nanogenerators, Adv. Funct. Mater. 29 (20) (2019), 1808820.
[145] M. Han, et al., Three-dimensional piezoelectric polymer microsystems for vibrational energy harvesting, robotic interfaces and biomedical implants, Nat. Electron. 2 (1) (2019) 26–35.
[146] E. Romero, R.O. Warrington, M.R. Neuman, Energy scavenging sources for biomedical sensors, Physiol Meas 30 (9) (2009) R35–R62.
[147] N. Lajnef, N.G. Elvin, S. Chakrabartty, A piezo-powered floating-gate sensor array for long-term fatigue monitoring in biomechanical implants, IEEE Trans. Biomed. Circuits Syst. 2 (3) (2008) 164–172.
[148] Y.R.J. Thomas, et al., A single sediment-microbial fuel cell powering a wireless telecommunication system, J. Power Sources 241 (2013) 703–708.
[149] X.A. Walter, et al., Scaling up self-stratifying supercapacitive microbial fuel cell, Int. J. Hydrogen Energy 45 (46) (2020) 25240–25248.
[150] S. Bauer, et al., 25th anniversary article: a soft future: from robots and sensor skin to energy harvesters, Adv. Mater. 26 (1) (2014) 149–162.
[151] S.J.A. Koh, et al., Dielectric elastomer generators: how much energy can be converted? IEEE/ASME Trans. Mechatron. 16 (1) (2010) 33–41.
[152] C. Dagdeviren, et al., Conformal piezoelectric energy harvesting and storage from motions of the heart, lung, and diaphragm, in: Proceedings of the National Academy of Sciences of the United States of America 111, 2014, pp. 1927–1932.
[153] A. Zurbuchen, et al., Towards batteryless cardiac implantable electronic devices-the Swiss Way, IEEE Trans. Biomed. Circuits. Syst. 11 (1) (2017) 78–86.
[154] A. Haeberlin, et al., Successful pacing using a batteryless sunlight-powered pacemaker, Europace 16 (10) (2014) 1534–1539.
[155] A. Haeberlin, et al., The first batteryless, solar-powered cardiac pacemaker, Heart Rhythm. 12 (6) (2015) 1317–1323.
[156] M.P. Kummer, et al., OctoMag: an electromagnetic system for 5-DOF Wireless Micromanipulation, IEEE Trans. Rob. 26 (6) (2010) 1006–1017.
[157] L. Zhang, K.E. Peyer, B.J. Nelson, Artificial bacterial flagella for micromanipulation, Lab Chip 10 (17) (2010) 2203–2215.
[158] S. Martel, et al., Adapting MRI systems to propel and guide microdevices in the human blood circulatory system, Conf. Proc. IEEE Eng. Med. Biol. Soc. 2004 (2004) 1044–1047.
[159] J.B. Mathieu, et al., MRI systems as a mean of propulsion for a microdevice in blood vessels, in: Proceedings of the 25th Annual International Conference of the IEEE Engineering in Medicine and Biology Society (IEEE Cat. No.03CH37439), Cancun, Mexico, 2003, pp. 3419–3422.
[160] J.B. Mathieu, G. Beaudoin, S. Martel, Method of propulsion of a ferromagnetic core in the cardiovascular system through magnetic gradients generated by an MRI system, IEEE Trans Biomed Eng 53 (2) (2006) 292–299.
[161] P. Vartholomeos, et al., MRI-guided nanorobotic systems for therapeutic and diagnostic applications, Annu Rev Biomed Eng 13 (2011) 157–184.
[162] S. Yin Chin, et al., Additive manufacturing of hydrogel-based materials for next-generation implantable medical devices, Sci Robot 2 (2) (2017) eaah6451.
[163] K.B. Yesin, K. Vollmers, B.J. Nelson, Modeling and control of untethered biomicrorobots in a fluidic environment using electromagnetic fields, Int. J. Robotics Res. 25 (5-6) (2016) 527–536.
[164] O. Ergeneman, et al., In vitro oxygen sensing using intraocular microrobots, IEEE Trans. Biomed. Eng. 59 (11) (2012) 3104–3109.
[165] S.M. Jeon, et al., A self-positioning and rolling magnetic microrobot on arbitrary thin surfaces, J. Appl. Phys. 115 (17) (2014) 17e303.
[166] H. Choi, et al., Two-dimensional actuation of a microrobot with a stationary two-pair coil system, Smart Mater. Struct. 18 (5) (2009), 055007.
[167] D. Kim, et al., Magnetic resonant wireless power transfer for propulsion of implantable micro-robot, J. Appl. Phys. 117 (17) (2015) 17e712.
[168] Z. Bi, et al., A review of wireless power transfer for electric vehicles: Prospects to enhance sustainable mobility, Appl. Energy 179 (2016) 413–425.
[169] M. T Nguyen, et al., Electromagnetic field based wpt technologies for uavs: A comprehensive survey, Electronics 9 (3) (2020) 461.
[170] M. Boyvat, J.-S. Koh, R.J. Wood, Addressable wireless actuation for multijoint folding robots and devices, Sci. Robot. 2 (8) (2017) eaan1544.
[171] G. Chatzipirpiridis, et al., Electroforming of implantable tubular magnetic microrobots for wireless ophthalmologic applications, Adv. Healthc. Mater. 4 (2) (2015) 209–214.
[172] C. Liu, et al., An effective sandwiched wireless power transfer system for charging implantable cardiac pacemaker, IEEE Trans. Ind. Electron. 66 (5) (2019) 4108–4117.